Remote Sensing of Environment 317 (2025) 114459

Contents lists available at ScienceDirect

Remote Sensing of Environment

journal homepage: www.elsevier.com/locate/rse

Two-decade surface ozone (O_3) pollution in China: Enhanced fine-scale estimations and environmental health implications

Zeyu Yang [a], Zhanqing Li [b,*], Fan Cheng [a], Qiancheng Lv [a], Ke Li [c], Tao Zhang [d], Yuyu Zhou [e,f], Bin Zhao [g,h], Wenhao Xue [i], Jing Wei [b,*]

[a] Faculty of Geographical Science, Beijing Normal University, Beijing, China
[b] Department of Atmospheric and Oceanic Science, Earth System Science Interdisciplinary Center, University of Maryland, College Park, MD, USA
[c] Jiangsu Key Laboratory of Atmospheric Environment Monitoring and Pollution Control, Collaborative Innovation Center of Atmospheric Environment and Equipment Technology, School of Environmental Science and Engineering, Nanjing University of Information Science and Technology, Nanjing, China
[d] Department of Geological and Atmospheric Sciences, Iowa State University, Ames, IA, USA
[e] Department of Geography, The University of Hong Kong, Hong Kong, China
[f] Institute for Climate and Carbon Neutrality, The University of Hong Kong, Hong Kong, China
[g] State Key Joint Laboratory of Environmental Simulation and Pollution Control, School of Environment, Tsinghua University, Beijing, China
[h] State Environmental Protection Key Laboratory of Sources and Control of Air Pollution Complex, Beijing, China
[i] School of Economics, Qingdao University, Qingdao, China

ARTICLE INFO

Editor: Menghua Wang

Keywords:
Surface ozone
Remote sensing
Deep learning
Urban-rural contrast
Exposure risk
Mortality burden

ABSTRACT

Surface ozone (O_3) has become a primary pollutant affecting urban air quality and public health in mainland China. To address this concern, we developed a nation-wide surface maximum daily average 8-h (MDA8) O_3 concentration dataset for mainland China (ChinaHighO_3) at a 10-km resolution with a start year of 2013, which has been widely employed in a wide range of studies. To meet the increasing demand for its usage, we have made important enhancements, including the development of a more advanced deep-learning model and the incorporation of major source updates, such as 1-km surface downward shortwave radiation and temperature directly from satellite retrievals, as well as a 1-km emission inventory. Additionally, we have extended the temporal coverage dating back to 2000, increased the spatial resolution to 1 km, and most importantly, notably improved the data quality (e.g., sample-based cross-validation coefficient of determination = 0.89, and root-mean-square error = 15.77 μg/m^3). Using the substantially improved new product, we have found dynamic and diverse patterns in national surface O_3 levels over the past two decades. Peak-season levels have been relatively stable from 2000 to 2015, followed by a sharp increase, reaching peak values in 2019 and subsequently declining. Additionally, we observed a large relative difference of 12 % in peak-season surface O_3 concentrations between urban and rural regions in mainland China. This disparity has greatly increased since 2015, particularly in the Beijing-Tianjin-Hebei and Pearl River Delta regions. Notably, since 2000, nearly all of the population across mainland China (> 99.7 %) has resided in areas exposed to surface O_3 pollution exceeding the World Health Organization (WHO) recommended long-term air quality guideline (AQG) level (peak-season MDA8 O_3 = 60 μg/m^3). Moreover, the short-term population-risk exposure to daily surface O_3 pollution has shown a significant increasing trend of 1.2 % ($p < 0.001$) of the days exceeding the WHO's recommended short-term AQG level (daily MDA8 O_3 = 100 μg/m^3) per year during the 22-year period. The overall upward trend (0.73 μg/m^3/yr, $p < 0.001$) in peak-season surface O_3 pollution has led to an exceptionally large rate of increase of 953 (95 % confidence interval: 486, 1288) premature deaths per year from 2000 to 2021 in mainland China. Urgent action is required to develop comprehensive strategies aimed at mitigating surface O_3 pollution to enhance air quality in the future.

* Corresponding authors.
E-mail addresses: zhanqing@umd.edu (Z. Li), weijing@umd.edu (J. Wei).

https://doi.org/10.1016/j.rse.2024.114459
Received 2 March 2024; Received in revised form 26 August 2024; Accepted 30 September 2024
Available online 21 November 2024

1. Introduction

Air pollution has arisen as a notable global environmental issue regarding both air quality and public health (GBD 2019 Risk Factors Collaborators, 2020). Ozone (O_3) is a naturally occurring component of the atmosphere, primarily concentrated in the stratosphere (~90 %), with its presence in the troposphere, especially near the Earth's surface, being relatively sparse (Lelieveld and Dentener, 2000; Wei et al., 2022a). The formation of O_3 is impacted by photochemical reactions involving diverse precursor substances, affected by both natural and anthropogenic factors. In the stratosphere, O_3 is crucial for absorbing harmful ultraviolet radiation, thereby safeguarding life on Earth. However, at the surface level, O_3, as a potent oxidant, adversely deteriorates air quality and disrupts ecological systems. Surface O_3 also directly harms vegetation, resulting in leaf damage, malformed fruits, decreased quality, and reduced agricultural output by causing cellular oxidation (Sadiq et al., 2017). More importantly, it presents a risk to public health by contributing to a range of diseases, potentially exacerbating or even triggering respiratory and cardiovascular conditions, such as asthma, stroke, hypertension, and inflammatory and coronary diseases (McConnell et al., 2002; Niu et al., 2022b; Soares and Silva, 2022), particularly impacting individuals with chronic obstructive pulmonary disease (COPD) (GBD 2019 Risk Factors Collaborators, 2020). The range of health issues arising from exposure to surface O_3 pollution not only exacerbates public health burdens but also inflicts important socio-economic losses (Czechowski et al., 2023; Maji et al., 2019).

Ozone pollution has had pronounced regional implications, especially in developing countries like China, where it has increased drastically in the last decade. From 2013 onwards, the government of China has implemented strong clean-air action plans to reduce anthropogenic emissions, which has successfully reduced fine particulate matter ($PM_{2.5}$) concentrations by 45.4 % (Wei et al., 2022a). On the other hand, surface O_3 concentration has significantly increased at an annual rate of 2.49 μg/m^3 per year ($p < 0.001$), offsetting the health benefit of air quality improvement gained from lowering $PM_{2.5}$ levels (Wei et al., 2021). The challenge of surface O_3 pollution in mainland China remains substantial, with ambient O_3 notably surpassing $PM_{2.5}$ as the primary pollutant impacting urban air quality (Li et al., 2021). To address this challenge, the Chinese government intensified its efforts in a nationwide campaign against pollution in 2021 by involving coordinated management of both O_3 and $PM_{2.5}$ pollution, with the objective of effectively controlling the upward trend of O_3 concentrations by 2025 (Lu et al., 2020a).

To date, numerous studies have been undertaken to estimate spatially continuous surface O_3 concentrations from space over China to minimize the impacts of insufficient spatial representation of ground-based observations, as well as the accuracy limitations from chemical transport model simulations (Wei et al., 2023a). Statistical models were initially employed for their flexible and practically applicable advantages (Mousavinezhad et al., 2021; Wang et al., 2023a). For instance, Mousavinezhad et al. (2021) employed a multiple linear regression (MLR) model to estimate daily maximum daily average 8-h (MDA8) O_3 concentrations between 2015 and 2019 at a spatial resolution of 10 km. Wang et al. (2023a) used a generalized additive model to derive daily O_3 concentrations from 2017 to 2019 across China at a spatial resolution of 0.1° × 0.1°. Although acceptable results can be obtained, it is very challenging for statistical models to construct robust conversion relationships for the estimation of surface O_3 due to the complexity of the underlying meteorological and chemical processes (Schlink et al., 2006).

Artificial intelligence (AI) has emerged as a promising new approach with strong data-mining capabilities, offering the advantage of simulating complex nonlinear processes and problems. A variety of machine- or deep-learning models has been adopted or extended for air pollutant modelling, including surface O_3 (Chen et al., 2021; Liu et al., 2020; Lyu et al., 2023; Meng et al., 2022; Mu et al., 2023; Taylan, 2017; Zhang et al., 2022; Zhu et al., 2022). For example, Liu et al. (2020) employed an eXtreme Gradient Boosting (XGBoost) algorithm to estimate daily surface O_3 concentrations in China between 2005 and 2017 at a horizontal resolution of 10 km. Mu et al. (2023) developed a three-dimensional Convolutional Neural Network (3D-CNN) architecture to estimate daily MDA8 O_3 concentrations (0.1° × 0.1°) from 2016 to 2020 across China. Our team has also retrieved daily surface O_3 concentrations from 2013 to 2020 in China at a 10-km resolution by employing an extended space-time extremely randomized trees (STET) model (Wei et al., 2022a). Note that all these products have coarse spatial resolutions (typically ≥10 km^2), limiting their applicability at fine urban scales. Specifically, they primarily focus on recent surface O_3 variations during relatively short study periods (especially since 2013). In addition, the Ministry of Ecology and Environment (MEE) of China only started collecting national ground-level O_3 observations after 2013. Studying the long-term spatiotemporal variations of national, regional, and city-level surface O_3 pollution in China is challenging mainly because of the scarcity of high-spatial-resolution historical records.

Surface O_3 is a great concern for human health, a topic increasingly being studied in China (Guan et al., 2021; Lu et al., 2020b; Lyu et al., 2023; Wang et al., 2021; Wang et al., 2022c; Wang et al., 2020b; Zhang et al., 2019; Zhang et al., 2022). Wang et al. (2020a) evaluated China's premature respiratory deaths resulting from prolonged exposure to surface O_3 pollution during a five-year period (2013–2017) and identified notable interannual fluctuations in both air pollution and mortality burden at various spatial scales, underscoring the importance of high-spatial-resolution data for more localized (urban) analyses. Wang et al. (2021) also noted that the sum of premature deaths due to long-term surface O_3 exposure has increased steadily by ~19.8 thousand people per year since 2013 in China. However, the scarcity of long-term surface O_3 data has led previous studies to concentrate on mortality in recent years (typically less than 10 years) related to O_3 exposure in China. Consequently, long-term trends of surface O_3 pollution, along with the resulting mortality-associated health effects, remain unclear over the past two decades in China.

Short-term surface O_3 exposure has garnered much attention due to its widespread impact on the population (Liu et al., 2019a, 2021; Orellano et al., 2020; Xiao et al., 2022). Zhang et al. (2022a) conducted a meta-analysis on short-term surface O_3 exposure in China and found that from 1990 to 2021, all-cause mortality, cardiovascular mortality, and respiratory mortality greatly increased, and surface O_3-attributed short-term all-cause deaths increased by 8.73 % from 2014 to 2020 (Zhang et al., 2022b). This growing emphasis on short-term assessments of daily O_3 exposure and its correlation with mortality risk underscores the critical need for spatially continuous daily data. There is thus a pressing need to obtain long-term, daily, gapless (complete spatial coverage) surface O_3 data at an elevated spatial resolution, which would facilitate detailed investigations at a finer scale when assessing the effects of surface O_3 exposure on both air quality and public health.

Questions to ask are: What were the distributions of surface O_3 concentrations, and how have they evolved over the last two decades? What are their impacts on public health concerning both long-term and short-term exposure to surface O_3 pollution? To address these questions, we reconstructed a 22-year (from 2000 to 2021) daily surface O_3 concentration dataset covering mainland China, which is spatially gapless (100 %) and has a high spatial resolution of 1 km. This dataset was derived from ground-based surface O_3 measurements and satellite retrievals of surface solar radiation and temperature, using a refined deep-forest model that considers multi-dimensional spatiotemporal information combined with meteorological parameters, an atmospheric reanalysis, and an emission inventory. The model's performance was rigorously accessed through 10-fold cross-validation and independent validation approaches. This unique dataset enables the comprehensive analysis of two-decade-long spatiotemporal O_3 variations, population-exposure risk, as well as the mortality burden, a dual perspective encompassing both long-term and short-term outlooks at each 1-km^2 grid across mainland China. Last, the distinct advantages of the finer-

resolution data are highlighted through a comparison with coarse-resolution data, focused on air quality and public health applications.

2. Materials and methods

2.1. Surface O_3 observations

Here, we used hourly ground-level O_3 data from two different terrestrial networks. One was sourced from the MEE, serving as the ground truth input for our deep-learning model to derive surface O_3 concentrations. These data (unit: μg/m^3) are observed at ~1630 monitoring stations (marked as blue dots in Fig. S1) every hour (recorded at local time) under standard conditions (273 K, 1013 hPa), starting in 2013. However, starting from 31 August 2018 onward, they were adjusted to room temperature and pressure conditions, i.e., 298 K and 1013 hPa. To maintain consistency in O_3 measurements, we scaled the newly measured values by a factor of 1.09375 to align them with the same standard conditions (MEE, 2018; Wei et al., 2022a).

The second source of data came from the Tropospheric Ozone Assessment Report (TOAR) database, which was not used as ground truth for model training but for independent validation purposes only. TOAR boasts the world's largest collection of tropospheric O_3 data, collecting long-term surface O_3 measurements from over 10,000 stations globally. There are four TOAR ground monitoring stations located in China, strategically positioned in both eastern and western regions, providing hourly observations since 1994 (marked as red dots in Fig. S1). Note that TOAR surface O_3 measurements are recorded in ppb at Coordinated Universal Time (UTC). We thus adjusted TOAR observations to ensure consistency with MEE measurements (MEE, 2018), including a time zone change (from UTC to local time) and a unit conversion (from ppb to μg/m^3) under standard conditions (i.e., 273 K and 1013 hPa). Additionally, MDA8 O_3 concentrations from MEE and TOAR were computed for each monitoring station in mainland China, following the quality control procedures described in our previous study (Wei et al., 2022a).

2.2. Refined ChinaHighO_3 framework

The ChinaHighO_3 dataset refers to the high-spatial-resolution (10 km) and high-data-quality [with an average sample-based (station-based) coefficient of determination (R^2) of 0.87 (0.80) and root-mean-square error (RMSE) of 17.10 (21.10) μg/m^3] daily surface MDA8 O_3 data in mainland China covering the period 2013–2020, part of the ChinaHighAirPollutants (CHAP) series. It was generated using an extended ensemble-learning approach known as the STET model (Wei et al., 2022a). In this study, we have refined the ChinaHighO_3 framework by implementing several major improvements: replacing the core STET model with an advanced four-dimensional spatiotemporal deep forest (4D-STDF) model, enhancing the spatial resolution from 10 km to 1 km with key high-resolution input variables, and extending daily data records back to 2000 (Table 1). Additionally, using this two-decade (2000−2021), high-temporal-resolution (daily), and high-spatial-resolution (1 km) gapless (spatial coverage = 100%) surface MDA8 O_3 dataset, we assessed both long-term trends in air quality and the associated (especially short-term) health impacts.

2.2.1. Model enhancements

Instead of conventional machine-learning models, this study employed a more advanced deep-learning model, i.e., deep forest (DF), showcasing a stronger data mining capability. DF uses the Multi-Grained Scanning approach to capture features and generate new input characteristics. It combines hierarchical decision trees to capture complex data patterns, beginning with base layers of decision trees from Random Forests and Extra Trees. These are then stacked in a cascade forest structure across multiple training layers. The results from these layers are finally integrated using an advanced model, such as the Forest,

Table 1
Comparison of models, variables, and accuracy between the old and new frameworks for estimating surface ozone in China.

Category		Old Framework			New Framework		
Model	Model name	Space-time extremely randomized trees (STET)			Four-dimensional spatiotemporal deep forest (4D-STDF)		
	Space information	Haversine great-circle distances			Euclidean spherical coordinates		
	Time information	Day of the year			Helix-shape trigonometric vectors		
	Variable	**Spatial resolution**	**Temporal resolution**	**Data sources**	**Spatial resolution**	**Temporal resolution**	**Data sources**
Input variables	Ozone (O_3) measurements	In situ	Hourly	MEE	In situ	Hourly	MEE and TOAR
	Downward shortwave radiation (DSR)	0.1°	Hourly	ERA5	1 km	3-h	MCD18A1
	Temperature (TEM)	0.1°	Hourly	ERA5	1 km	Daily	Global seamless land surface temperature dataset
	Emission inventory (NO_X, VOCs, CO)	0.25°	Monthly	Multiresolution Emission Inventory for China (MEIC)	1 km	Daily	Air Benefit and Cost and Attainment Assessment System-Emission Inventory (ABaCAS-EI) v2.0
	Temporal range	2013–2020			2000–Present		
	Spatial resolution	10 km			1 km		
Product	Overall Accuracy	CV-R^2 = 0.87 RMSE = 17.10 μg/m^3			CV-R^2 = 0.89 RMSE = 15.77 μg/m^3		
	Predictive ability	CV- R^2 = 0.80 RMSE = 21.10 μg/m^3			CV-R^2 = 0.84 RMSE = 18.74 μg/m^3		

XGBoost, or LightGBM (Zhou and Feng, 2019). In our study, hyperparameter optimization was conducted using a loop iteration method. Optimal settings include the number of estimators in each cascade layer set to 4, the number of trees in each estimator set to 100, no maximum depth for each tree, and the type of predictor concatenated to the DF being LightGBM. Compared with machine-learning and other neural-network-derived deep-learning models, it offers unique advantages, including local perception, parameter sharing, spatial invariance, feature extraction, and automatic learning. It is particularly notable for requiring a smaller number of hyperparameters and adjustments, demonstrating proficiency in effectively handling data-intensive tasks (Anghel et al., 2018; Liu et al., 2019b).

Apart from improving the model, we have made important improvements in capturing spatiotemporal information about air pollution during the modelling process. Considering the unequal impact of air pollution variations over both space and time, we departed from using the previously employed direct great-circle distances between spatial points. Instead, we adopted a similar polar coordinate form to distinguish their spatiotemporal similarities and differences more accurately, leading to an improved 4D-STDF model (Wei et al., 2023a). The space factor is denoted by three Euclidean spherical coordinates [S_1, S_2, and S_3], which are functions of the geographical coordinates, namely, longitude (*Lon*) and latitude (*Lat*) (Eqs. 1–3). The time factor is represented by three helix-shape trigonometric vectors [T_1, T_2, and T_3], which are functions of the day of the year (*DOY*) and the complete count of days within a single year (*N*) (Eqs. 4–6), capturing temporal variations and particularly emphasizing seasonal cycles.

$$S_1 = sin\left(2\pi\frac{Lon}{360}\right) \tag{1}$$

$$S_2 = cos\left(2\pi\frac{Lon}{360}\right)sin\left(2\pi\frac{Lat}{180}\right) \tag{2}$$

$$S_3 = cos\left(2\pi\frac{Lon}{360}\right)cos\left(2\pi\frac{Lat}{180}\right) \tag{3}$$

$$T_1 = \frac{DOY}{N} \tag{4}$$

$$T_2 = cos\left(2\pi\frac{DOY}{N}\right) \tag{5}$$

$$T_3 = sin\left(2\pi\frac{DOY}{N}\right) \tag{6}$$

2.2.2. Data source updates

We have updated the major input predictors to a higher spatial resolution of 1 km for estimating surface O_3 concentrations compared to our previous study that generated data at a 10-km resolution (Wei et al., 2022a). Specifically, we replaced the two key meteorological variables, surface downward shortwave radiation (DSR) and air temperature (TEM)—which contributed 32 % and 14 %, respectively, to the estimation of surface O_3 via photochemical reactions (Wei et al., 2022a)—from the coarse-resolution (0.1° × 0.1°) European Centre for Medium-Range Weather Forecasts Reanalysis v5 (ERA5) global reanalysis with newly released Moderate Resolution Imaging Spectroradiometer (MODIS) 1-km-resolution DSR (Wang et al., 2020a) and land surface temperature (LST) (Zhang et al., 2022c) products. Additionally, we updated the three main anthropogenic emissions of O_3 precursors (i.e., NO_X, VOCs, CO) by replacing the monthly Multi-resolution Emission Inventory for China (MEIC) dataset (0.25° × 0.25°) with the daily Air Benefit and Cost and Attainment Assessment System-Emission Inventory (ABaCAS-EI) dataset at a 1-km resolution (Li et al., 2023). In addition to the increased computational power, the improvements in input variables allow us to enhance surface O_3 estimates from a 10-km to 1-km resolution.

Other variables remained the same as our previous study, including main meteorological variables, i.e., boundary-layer height, relative humidity, horizontal and vertical winds, surface pressure, evaporation, and precipitation, obtained from the ERA5 reanalysis (0.1° to 0.25°), as well as land-surface- and population-related features, including the normalized difference vegetation index (1 km), surface elevation (90 m), and population distribution (1 km), provided by MODIS, the Shuttle Radar Topography Mission (SRTM), and LandScan™, respectively. Finally, we aggregated or resampled all variables to maintain a consistent resolution of 1 km with the main predictors using a bidirectional interpolation approach. Fig. 1 shows the flowchart of our updated ChinaHighO_3 framework.

2.3. Population-exposure risk assessment

Both long-term and especially short-term exposures to surface O_3 pollution are linked to heightened risks of disease and mortality (Bell et al., 2004; Turner et al., 2015). The World Health Organization (WHO) has issued recommended air quality guidelines (AQGs) since 1987 with the aim of promoting healthy air to optimize both air quality and health benefits. The most recent version, updated in September 2021, recommends two long-term interim targets (L-IT1 and L-IT2) and one AQG (L-AQG) level with peak-season MDA8 O_3 concentrations (six consecutive months with the highest six-month running-average O_3 concentration according to WHO's definition) of 100, 70, and 60 μg/m^3, respectively. There are also three similarly recommended short-term air quality standards (S-IT1, S-IT2, and S-AQG), with daily MDA8 O_3 concentrations set at 160, 120, and 100 μg/m^3, respectively.

Here, we evaluated the population-risk exposure to long-term and short-term surface O_3 pollution according to the WHO-recommended air quality guidelines. For the prolonged O_3 exposure risk assessment, we computed the annual percentage of populated areas where the peak-season population-weighted MDA8 O_3 value exceeded the WHO's recommended long-term air quality standards, along with the proportions of the population residing in polluted areas (i.e., population density > 0). In the case of the short-term O_3 exposure risk assessment, we calculated the percentage of days where the daily population-weighted MDA8 O_3 value surpassed the short-term air quality standards recommended by WHO within one year at each 1-km^2 grid across mainland China.

2.4. Mortality burden estimation

Both long-term and short-term exposures to surface O_3 pollution have important health impacts, e.g., COPD, as evidenced by many studies (GBD 2019 Risk Factors Collaborators, 2020). To assess the mortality burden induced by long-term surface O_3 exposure, we used a log-linear exposure-response function from the Global Burden of Disease (GBD) study (GBD 2019 Risk Factors Collaborators, 2020), i.e., the relative risk (RR) for mortality is 1.061 [95 % confidence interval (CI): 1.029–1.093] with an increase in peak-season MDA8 O_3 concentration per 10 ppb. Premature deaths resulting from long-term O_3 exposure can then be estimated as follows:

$$LD_{g,y} = \left(1 - 1/RR_{j,g}\right) \times Pop_{g,y} \times B_y \tag{7}$$

where $LD_{g,y}$ refers to the cumulative fatality count (unit: people) attributed to long-term O_3 exposure in grid *g* in year *y*; $RR_{g,j}$ represents the RR at exposure level *j* in grid *g* relative to the population exposed to above the theoretical minimum-risk exposure level (29.1–35.7 ppb); $Pop_{g,y}$ denotes the population in grid *g* in year *y*, provided by the annual LandScan™ population distribution (1 km) product; and B_y signifies the baseline mortality rate of COPD in year *y* in China, collected from the GBD database.

For acute health impacts, we used the log-linear exposure-response function derived from a nationwide representative large cohort study in

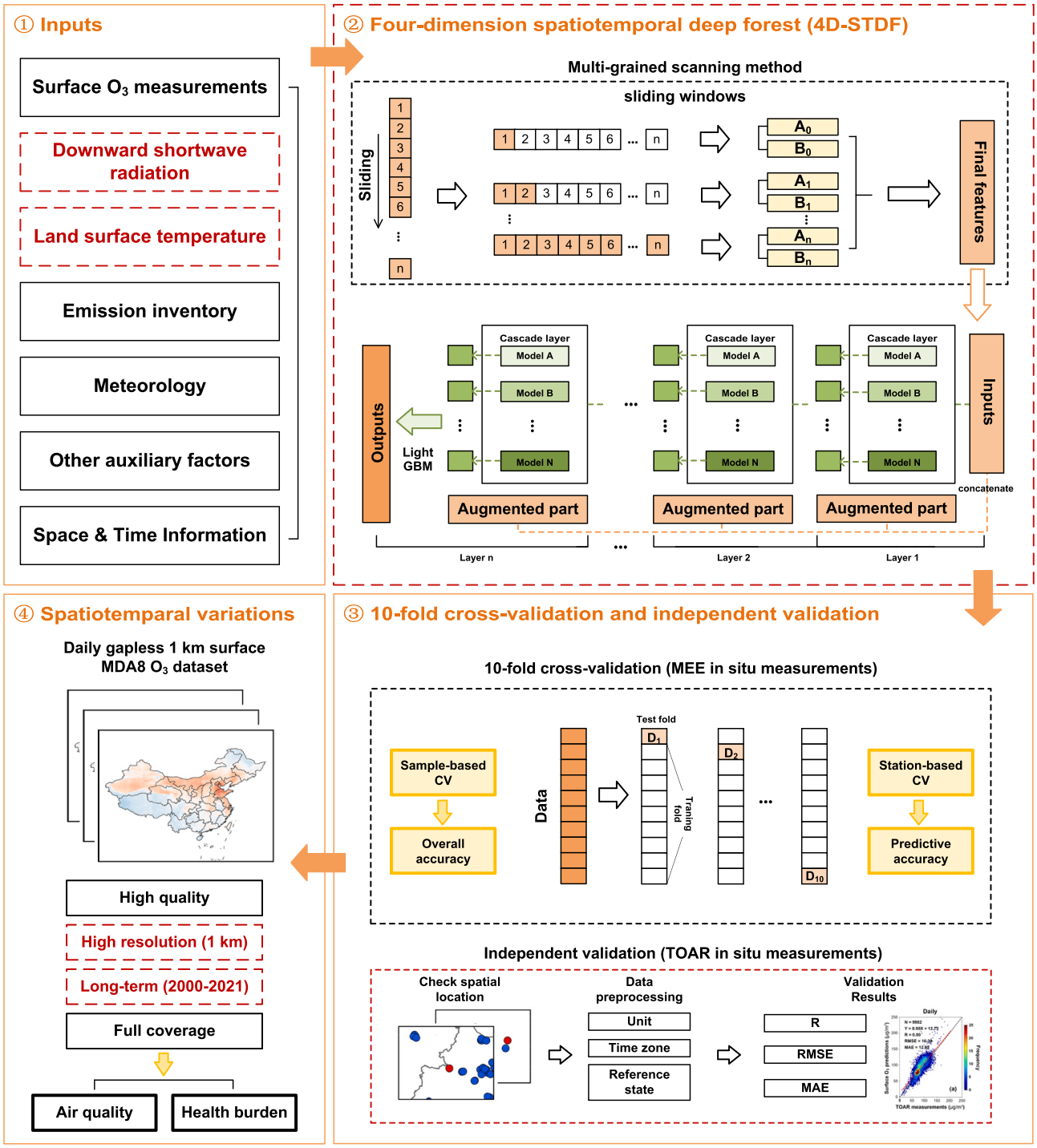

Fig. 1. Flowchart of the updated ChinaHighO_3 framework in this study (text in red and dotted boxes highlight the main steps that were improved, encompassing the inputs, model, and validation). (For interpretation of the references to colour in this figure legend, the reader is referred to the web version of this article.)

China, i.e., the RR for mortality is 1.0024 (95 % CI: 1.0013–1.0035) with every 10 ppb rise in daily MDA8 O_3 concentration (Yin et al., 2017). The mortality burden due to short-term surface O_3 exposure in one day can then be calculated using the daily MDA8 O_3 concentration and classic risk assessment method (Guan et al., 2021):

$$SD_{g,d} = \left(1 - 1/RR_{j,g}\right) \times Pop_{g,y} \times \left(\frac{B_y}{365}\right) \quad (8)$$

where $SD_{g,d}$ refers to the number of mortalities resulting from short-term surface O_3 exposure within a specific grid g on a particular day d. The term $RR_{g,j}$ indicates the effect estimates for the population at exposure level j in grid g. Pop_i denotes the population in grid g for year y, and the expression (B_y/365) represents the daily baseline of total mortality rate in grid g.

2.5. Validation and analysis methods

We assessed the model's performance by using the common 10-fold cross-validation (10-CV) method and independent validation approaches. Initially, we used the widely used sample-based (out-of-sample) 10-CV procedure to verify the overall accuracy of the model (i.e.,

dividing data samples into 10 folds, where 1 fold is for validation and the other 9 folds are for training) using MEE measurements from 2013 to 2021 (Wei et al., 2022a). Furthermore, we employed an additional station-based (out-of-station) 10-CV approach by randomly dropping MEE stations for validation to assess the model's spatial predictive ability in areas where no ground measurements were available (Table 1). Specifically, this approach randomly divides all MEE monitoring stations in mainland China into 10 equally sized groups. In each CV iteration, data samples from 9 groups (90 % of the stations) are used for training, while data samples from the remaining group (10 % of the stations) are used for independent validation. This process was repeated 10 times, ensuring that each station's measurements serve as validation data once.

Studying long-term air pollution trends relies heavily on the quality of historical records, particularly when ground-based observations are lacking before 2013. Independent validation against other ground-truth sources helps identify potential errors or discrepancies (Oberkampf and Roy, 2010). Therefore, measurements from the TOAR network were employed to independently validate our surface O_3 predictions before 2013, when MEE measurements were unavailable. Additionally, we conducted an independent validation following our previous approach (Wei et al., 2021). Specifically, we trained our model using data samples from post-2016 and then predicted surface O_3 levels for the years 2015, 2014, and 2013 separately. These predictions were subsequently validated against ground measurements from the corresponding years, sourced from 1480, 945, and 945 monitoring stations, respectively, across mainland China.

We used the population-weighted surface O_3 concentration to evaluate the exposure risk and mortality burden from surface O_3 pollution, expressed as:

$$C_{pw,g} = \frac{\sum_{i=1}^{n}\left(C_g \times Pop_{g,y}\right)}{\sum_{i=1}^{n} Pop_{g,y}} \quad (9)$$

where $C_{pw,g}$ represents the population-weighted O_3 concentration within grid g, and $C_{g,y}$ and $Pop_{g,y}$ represent the surface O_3 concentration and population in the same grid g, respectively. Furthermore, we used monthly surface O_3 anomalies by removing seasonal cycles to calculate temporal trends through the approach of linear regression using the least-squares method, then assessed the confidence levels of the estimated trends to determine their significance using the two-sided hypothesis test method (Wei et al., 2019).

In this research, we integrated an analysis of temporal series with a sliding window (spanning at least 12 months) approach to identify breakpoints during the long-term period when a reverse trend emerged, following the approach adopted in our previous study (Wei et al., 2023a). This can pinpoint the greatest level of change in opposing directions in trends before and after the breakpoint by assessing both the magnitude of the change and the probability of statistical significance of trends on either side of the potential breakpoint. Here, we considered the statistical significance beyond a 90 % confidence level ($p < 0.1$) on at least one side.

3. Results and discussion

3.1. Model validation and comparison

We first evaluated the model's overall accuracy using ~4.2 million data samples gathered from 2013 to 2021 in mainland China, employing an out-of-sample (sample-based) 10-CV approach (Table 2). Validation results show that our model can estimate daily MDA8 O_3 concentrations more accurately across different years, as evidenced by increasing cross-validation R^2 (CV-R^2) values ranging from 0.79 to 0.94 and decreasing RMSE [mean absolute error (MAE)] values from 22.56 (14.64) to 10.62 (7.39) μg/m^3. This is attributed to the increase in the density of site observations and the growth in sample size over time, thereby enhancing the model's training capabilities and overall accuracy. In general, our 1-km daily MDA8 O_3 estimates and surface measurements are highly consistent, with an average CV-R^2 of 0.89 and RMSE (MAE) value of 15.77 (10.48) μg/m^3 (Fig. 2a). The station-based CV results demonstrate a strong spatial predictive ability, with an increase in CV-R^2 from 0.68 to 0.93 and a decrease in RMSE (MAE) from 28.45 (19.22) to 11.39 (7.91) μg/m^3 over the years from 2013 to 2021 (Table 2). This improvement is mostly attributed to the increasing number of ground observations across mainland China. On average, the CV-R^2 is 0.84, with an RMSE (MAE) value of 18.74 (12.36) μg/m^3, respectively (Fig. 2c). This illustrates the model's robustness in predicting surface O_3 levels in areas lacking ground-based measurement data. The accuracy of monthly and annual estimates and predictions has continuously improved during the period 2013–2021 (Fig. 2). Additionally, we evaluated the model performance by creating residual histograms to compare our MDA8 O_3 retrievals with MEE observations across various temporal scales. In general, the histograms of their differences show normal distributions across daily, monthly, and peak-season scales. Specifically, 80 % of the residuals fall within ± 16, ± 10, and ± 8 μg/m^3, respectively (Fig. S2a-c). Similar findings are observed for our MDA8 O_3 predictions, where nearly 80 % of them demonstrate high consistency with observations, with residuals of ± 19 μg/m^3, ± 13 μg/m^3, and ± 8 μg/m^3 at the three temporal scales, respectively (Fig. S2d-f).

Furthermore, we evaluated the model performance in retrieving daily MDA8 O_3 levels across five major sub-areas in mainland China (Table S1). The overall accuracy is consistently reliable across all regions, with sample-based CV-R^2 values exceeding 0.85 and RMSE and MAE values below 19 and 13 μg/m^3, respectively. Performance is notably strong in the Beijing-Tianjin-Hebei (BTH) region (CV-R^2 = 0.92, RMSE = 16.64 μg/m^3). Our model also demonstrates robust spatial predictive ability in most regions, with station-based CV-R^2 values greater than 0.83 and small uncertainties (i.e., RMSE = 19–21 μg/m^3,

Table 2
The 10-fold CV results of MDA8 O_3 concentrations (μg/m^3) at a 1-km resolution for each year from 2000 to 2021 in mainland China. The values in parentheses represent the percentage change compared to the validation results of CHAP O_3 at a 10-km resolution.

	Overall accuracy			Spatial predictive ability		
Year	**R^2**	**RMSE**(μg/m^3)	**MAE**(μg/m^3)	**R^2**	**RMSE**(μg/m^3)	**MAE**(μg/m^3)
2013	0.79 (↑0.1)	22.56 (↑2.6)	14.46 (↓2.5)	0.68 (↑7.4)	27.96 (↓5.4)	18.80 (↓5.1)
2014	0.81 (↑1.6)	22.26 (↓0.6)	14.64 (↓1.2)	0.69 (↑6.4)	28.45 (↓5.2)	19.22 (↓6.3)
2015	0.81 (↑2.0)	20.62 (↓1.3)	13.98 (↑0.6)	0.70 (↑8.6)	25.75 (↓7.2)	17.72 (↓6.1)
2016	0.84 (↑2.3)	18.08 (↓5.8)	12.54 (↓3.5)	0.77 (↑6.5)	21.69 (↓8.5)	15.28 (↓6.7)
2017	0.90 (↑1.4)	14.69 (↓5.3)	10.45 (↓3.2)	0.87 (↑2.8)	16.69 (↓6.3)	11.93 (↓4.9)
2018	0.92 (↑1.2)	13.13 (↓6.9)	9.26 (↓4.0)	0.90 (↑2.5)	14.57 (↓7.0)	10.28 (↓5.0)
2019	0.93 (↑1.6)	13.00 (↓7.1)	9.07 (↓4.5)	0.92 (↑1.2)	14.24 (↓7.0)	9.95 (↓5.1)
2020	0.94 (↑1.2)	11.08 (↓7.4)	7.68 (↓3.6)	0.93 (↑1.1)	12.01 (↓7.3)	8.34 (↓4.2)
2021	0.94	10.62	7.39	0.93	11.39	7.91
2013–2020	0.88 (↑1.1)	16.52 (↓3.4)	11.03 (↓2.3)	0.83 (↑3.6)	19.75 (↓6.4)	13.14 (↓5.3)
2013–2021	0.89 (↑2.3)	15.77 (↓7.8)	10.48 (↓7.2)	0.84 (↑5.0)	18.74 (↓11.2)	12.36 (↓10.9)

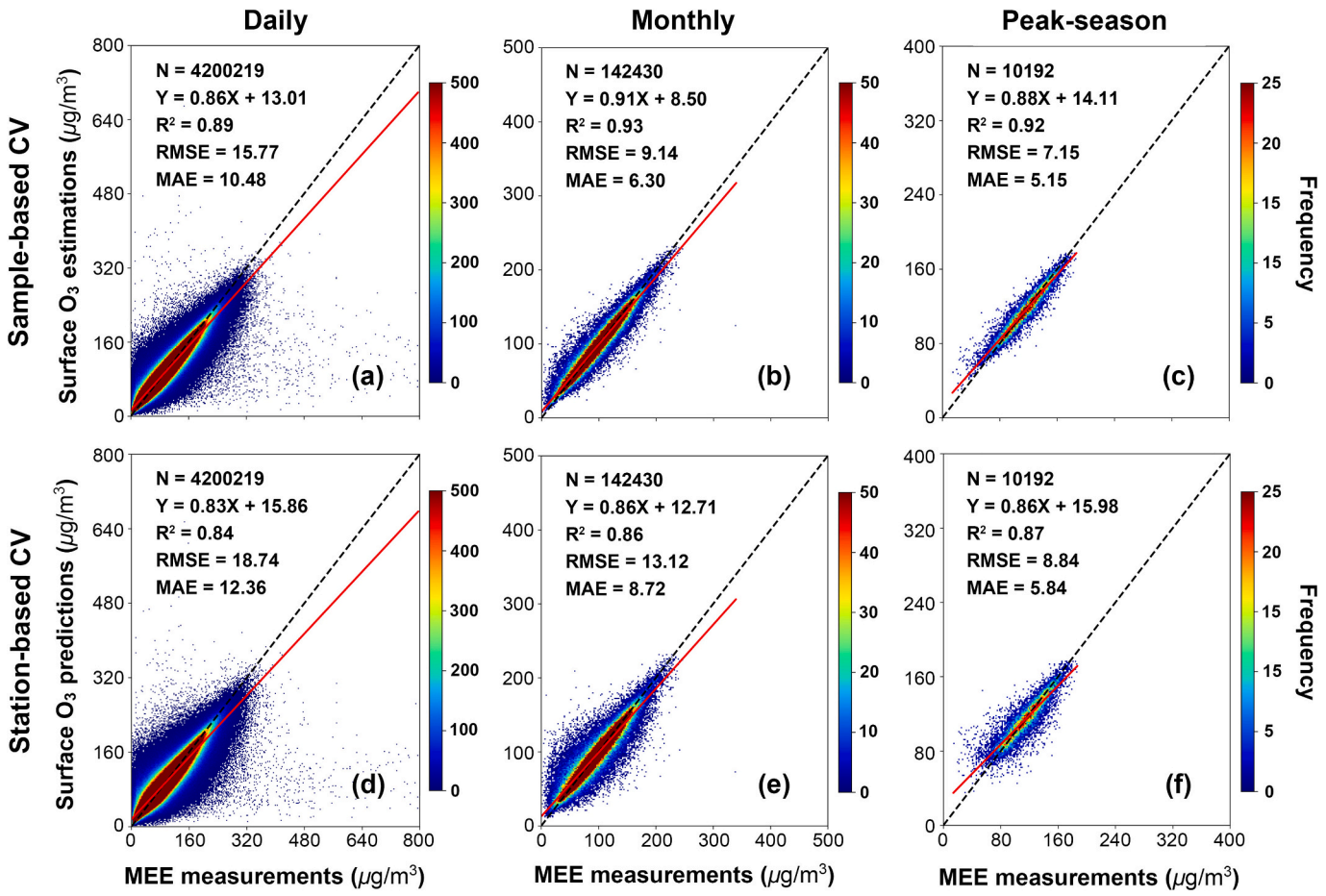

Fig. 2. Density scatter plots of sample-based (top row) and station-based (bottom row) 10-fold cross-validation (CV) outcomes for daily (left column), monthly (middle column), and peak-season (right column) surface O_3 retrievals in mainland China between 2013 and 2021. Dotted black lines represent 1:1 lines, and solid red lines indicate optimal-fit lines derived from linear regression. (For interpretation of the references to colour in this figure legend, the reader is referred to the web version of this article.)

and MAE = 12–15 μg/m^3). However, the model does not perform as well for the Tibetan Plateau, having the lowest CV-R^2 value of 0.62, primarily due to the sparsity of monitoring stations and the topographically complex natural environment.

Compared to 10-km data (Wei et al., 2022a), the 1-km data has an improved overall accuracy, with CV-R^2 values increasing from 0.1 % to 2.3 % (average = 1.1 %) and RMSE and MAE values decreasing from 0.6 % to 7.4 % (average = 3.4 %) and 0.6 % to 4.5 % (average = 2.3 %) over the years, respectively (Table 2). Similar continuous improvements in predictive accuracy are also observed from 2013 to 2020, with the average station-based CV-R^2 value increasing by 3.6 % and average RMSE and MAE values decreasing by 6.4 % and 5.3 %, respectively. These results illustrate that our updated framework not only achieves a tenfold increase in spatial resolution but also enhances the quality of the data. This high-resolution and high-quality data will be highly valuable in monitoring air pollution and assessing exposure risks on a finer scale, particularly within urban areas.

Additionally, we used TOAR long-term ground-based O_3 observations to validate our reconstructed data records before 2013. Unlike CV, we directly compared our satellite-based MDA8 O_3 retrievals with independent TOAR measurements at four monitoring stations in mainland China (Fig. 3a-c). This comparison involved 9982, 217, and 34 collocated samples at daily, monthly, and annual levels, respectively. Independent validation with TOAR measurements further illustrates the reliability of historical predictions on daily [correlation coefficient (R) = 0.80, RMSE = 16.39 μg/m^3], monthly (R = 0.89, RMSE = 15.16 μg/m^3), and annual (R = 0.90, RMSE = 10.39 μg/m^3) scales, especially for the period before 2013 when there were no MEE observations.

Furthermore, we tested our model performance in predicting historical surface O_3 concentrations for the years 2015, 2014, and 2013 separately, using a model trained on data samples from subsequent years (post-2016). The overall accuracy of our predictions, based on a total of 985,688 daily, 19,045 monthly, and 2889 annual collocated data samples for these years (2013–2015), remains reliable across different temporal scales: daily (R = 0.90, RMSE = 40.11 μg/m^3), monthly (R = 0.97, RMSE = 12.60 μg/m^3), and annual (R = 0.97, RMSE = 9.00 μg/m^3) (Fig. 3d-f). Importantly, our daily predictions consistently align with ground measurements in all evaluation indicators across different years. Specifically, we achieve the same R values of 0.9 and slopes greater than 0.8, with RMSE (MAE) values ranging from 38 (28) to 41 (30) μg/m^3 (Fig. S3). Similar conclusions can be observed in the monthly (R = 0.96–0.98, RMSE = 10–13 μg/m^3) and annual (R = 0.96–0.97, RMSE = 8–9 μg/m^3) composites. These findings demonstrate, in part, the overall robustness and stability of our model in reconstructing historical (pre-2013) surface O_3 concentrations. This suggests that the data samples used are large enough for the current application.

Although we have provided additional context through independent validations, the scarcity of ground-based measurements before 2013 suggests that our historical predictions still contain uncertainties and biases. This limitation underscores the need for future work to gather more comprehensive validation datasets to better assess the reliability of these historical predictions. It is also important to note that our input variables may have systemic discrepancies, particularly for the main inputs derived from MODIS products. For example, i.e., MODIS DSR

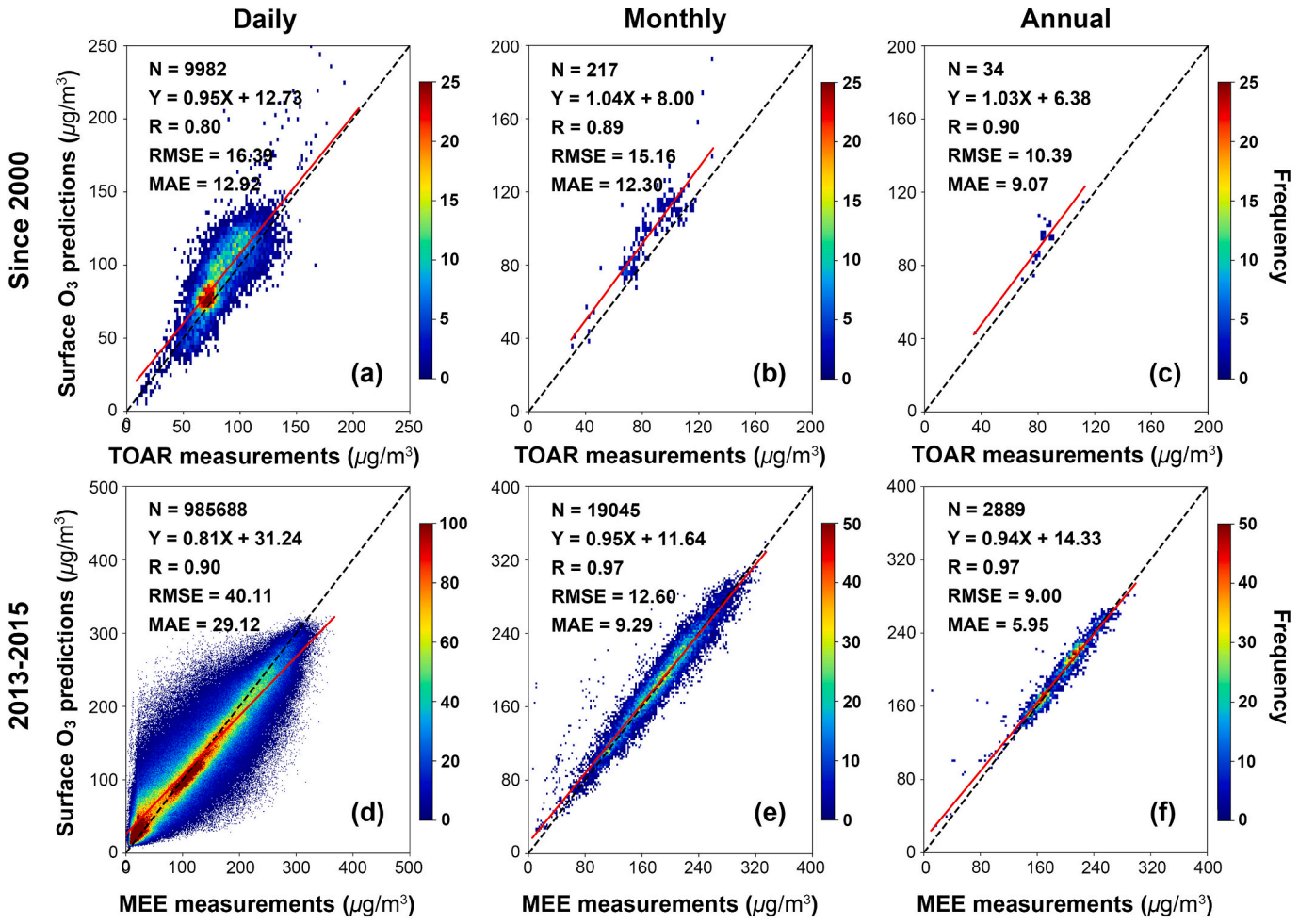

Fig. 3. Independent validations between our surface MDA8 O_3 predictions and (a-c) TOAR O_3 measurements from four monitoring stations since 2000, and (d-f) MEE O_3 measurements from 1480 unique monitoring stations during 2013–2015 in mainland China, at daily, monthly, and annual levels, respectively.

products have an average accuracy (R^2) of 0.86 with an RMSE value of 119.2 W/m^2 against field measurements (Wang et al., 2020a), while MODIS gap-filled LST products have average R^2 values ranging from 0.98 to 1 and RMSE values ranging from 1.33° to 1.88° for daytime and nighttime compared to ground measurements (Zhang et al., 2022c). These uncertainties can amplify during the model training process, potentially affecting the quality of our ChinaHighO_3 dataset.

3.2. *Spatiotemporal surface O_3 variations during 2000–2021*

Using the 4D-STDF model, we have generated seamless daily O_3 maps from 2000 to 2021 in mainland China with a 1-km spatial resolution. Fig. 4 illustrates the spatial distributions in peak-season surface O_3 concentrations in mainland China for each year over the past two decades. Over the 22-year span, most of northern China has consistently experienced elevated ambient O_3 levels surpassing 120 μg/m^3, with notable hot spots in the North China Plain (NCP) and Yangtze River Delta (YRD) region. However, in the southwest region of China and Heilongjiang province, surface O_3 pollution has remained comparatively lower (~80 μg/m^3). Temporally, surface O_3 concentrations underwent large fluctuations: from 2000 to 2016, they remained relatively stable, averaging between 92.6 ± 22.8 μg/m^3 to 95.5 ± 14.7 μg/m^3. The BTH (average = 116.5 ± 8.9 μg/m^3) and NCP (average = 115.3 ± 11.3 μg/m^3) regions exhibited more severe O_3 pollution, consistently surpassing 100 μg/m^3. This could potentially be attributed to the heavy industrial activity in northern areas, resulting in higher precursor emissions (Wei et al., 2022b). Conversely, the Pearl River Delta (PRD) (average = 88.0 ± 6.1 μg/m^3) experienced comparatively lighter O_3 pollution. However, a marked increase in O_3 concentration has been observed across mainland China since 2017, especially in the eastern and northern regions, where O_3 concentrations reached above 120 μg/m^3, highlighting the challenge in further improving the air quality in China (Hashim et al., 2021; Zhao et al., 2022b). The year 2019 recorded the highest O_3 concentrations, averaging 114.9 ± 17.8 μg/m^3 across mainland China, with more severe conditions observed in the NCP (~153.8 ± 10.7 μg/m^3) and BTH (~147.1 ± 17.8 μg/m^3) regions. Additionally, the PRD (~102.8 ± 7.0 μg/m^3) surpassed the 100 μg/m^3 mark for the first time after 2000. After 2019, a decline in nationwide O_3 pollution was seen, notably prominent in the NCP region. Tibet has shown a more dramatic increase in surface O_3 concentrations between 2016 and 2021 compared to other provinces, also noted in previous studies (Chen et al., 2022b; Yin et al., 2022). More frequent stratosphere-troposphere exchange events primarily lead to stratospheric O_3 intrusions and substantial increases in local surface O_3 pollution (Liu et al., 2022a; Yang et al., 2022; Yin et al., 2023) despite the relatively low levels of O_3 precursors (e.g., NO_x and VOCs). In addition, the high altitude, low latitude, and extensive snow cover of the Tibetan Plateau result in intense solar radiation (Lin et al., 2008), which, along with the long-range transport of various pollutants, further promotes O_3 formation (Xu et al., 2018).

To delve deeper into the long-term variations in surface O_3 concentrations, we calculated the temporal trends of MDA8 O_3 from 2000 to 2021 at both seasonal and annual (specifically, peak-season) scales (Fig. S4). In general, 97 % of the regions showed an increasing annual trend,

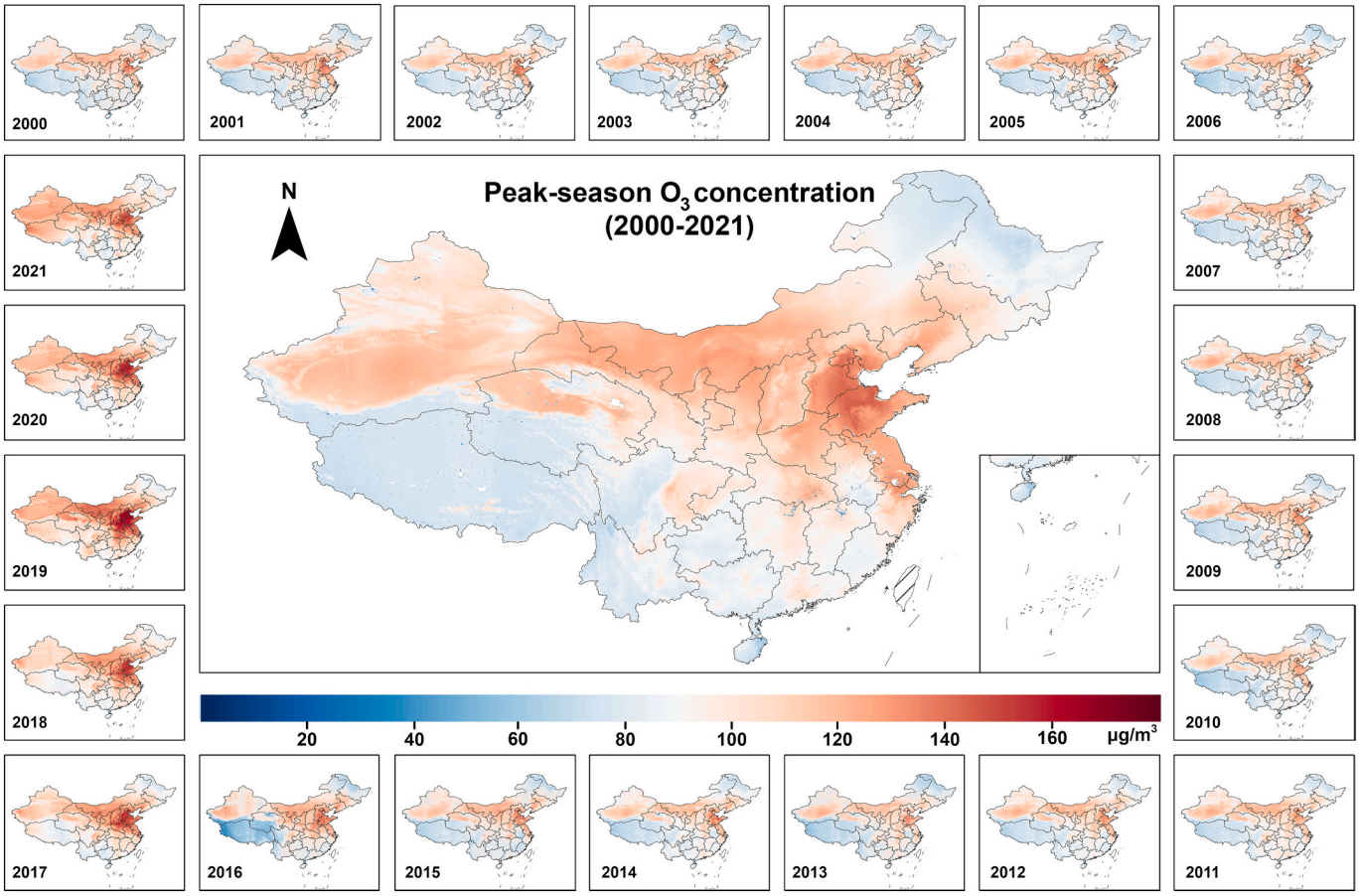

Fig. 4. Average peak-season surface O_3 maps at a 1-km resolution spanning 2000 to 2021 for mainland China. The central map shows the 22-year average, and smaller maps surrounding it show maps for each individual year.

with the largest increases (> 2 μg/m^3/yr, $p < 0.05$) concentrated in southeastern regions and areas adjacent to the Central China Plain (Fig. S4a). This trend, particularly evident after 2016, recorded a substantial increase of 3.77 μg/m^3/yr ($p < 0.001$). Differences exist at seasonal levels: In spring (Fig. S4b), there was an upward trend in O_3 concentration over the largest expanse, covering ~98 % of the country's regions. Additionally, the springtime trend did not change much before 2014, when a modest increase began in 2014 (3.37 μg/m^3/yr, $p < 0.001$). Among the four seasons, summertime O_3 showed the strongest upward trend, especially notable since 2016 (4.05 μg/m^3/yr, $p < 0.001$) and particularly evident in the NCP region (Fig. S4c). In autumn (Fig. S4d), the annual trend in O_3 variations showed an increasing trend over most of mainland China (~90 %), with decreasing trends observed in the northeast and southwest regions. By contrast, O_3 pollution was at its lowest in winter (average = 65.3 ± 5.3 μg/m^3; ~1.5 times lower than in summer). Similarly, a slightly increasing trend occurred in most parts of eastern China. A shorter duration of sunlight and lower temperatures in winter in the Northern Hemisphere hinder surface O_3 production.

To further investigate the dynamic and diverse patterns in surface O_3 pollution over the past two decades, we plotted the time series of monthly O_3 anomalies for mainland China and each typical region (Fig. 5). Throughout the study period (2000–2021), a noticeable rise in population-weighted O_3 concentrations was observed in mainland China (0.73 μg/m^3/yr, $p < 0.001$) and three key urban regions, i.e., BTH (0.93 μg/m^3/yr, $p < 0.001$), YRD (0.80 μg/m^3/yr, $p < 0.001$), and PRD (0.54 μg/m^3/yr, $p < 0.001$) (Fig. 5b-d). This is linked to rapid industrialization and urbanization, accompanied by a widespread surge in the release of O_3 precursor emissions, specifically VOCs and NO_X, from vehicles, industries, and power plants (Yang et al., 2023; Zeng et al., 2019). However, the trends differed, or even became opposite, during subperiods at both national and regional levels. In mainland China, surface O_3 levels remained relatively stable until about 2015, after which O_3 levels experienced a sharp increase (4.36 μg/m^3/yr, $p < 0.001$), reaching a peak in 2019, followed by a subsequent decline (−1.95 μg/m^3/yr, $p < 0.05$). Similarly, yet with distinct nuances, the three key regions initially experienced overall declines persisting until 2014, except for PRD (where the decrease continued until 2016), followed by substantial increases across all regions observed until 2019. One potential reason for the recent increase in O_3 levels is the continuous decrease in NO_2 concentrations in recent years (Anenberg et al., 2022; Wei et al., 2022b), facilitating the accumulation of O_3 in the atmosphere. Another notable decline was observed in most regions in China (Wang et al., 2023b), particularly evident in BTH with a decrease of 6.71 μg/m^3 per year ($p < 0.01$), while PRD exhibited an exception with an increase of 1.63 μg/m^3 per year. This is attributed to reduced emissions of O_3 precursors during the COVID-19 lockdowns in 2020 (Adame et al., 2022), coupled with the ongoing implementation of continuous air quality protection policies by the Chinese government (Ren et al., 2022). Note that the "2 + 26" cities (i.e., BTH and surrounding cities) situated within the core of the NCP exhibited the largest increase during the entire period (1.14 μg/m^3/yr, $p < 0.001$). This increase was particularly prominent for the period 2016–2019 (6.02 μg/m^3/yr, $p < 0.01$). However, these cities demonstrated the smallest decrease (−4.74 μg/m^3/yr, $p < 0.05$) in the subsequent period of 2020–2021 (Fig. 5e-f), highlighting the severity of O_3 pollution in urban areas.

The distinct advantage of 1-km data enables us to examine the differences and variations in peak-season O_3 concentration between urban and rural areas in mainland China using the annual urban extents

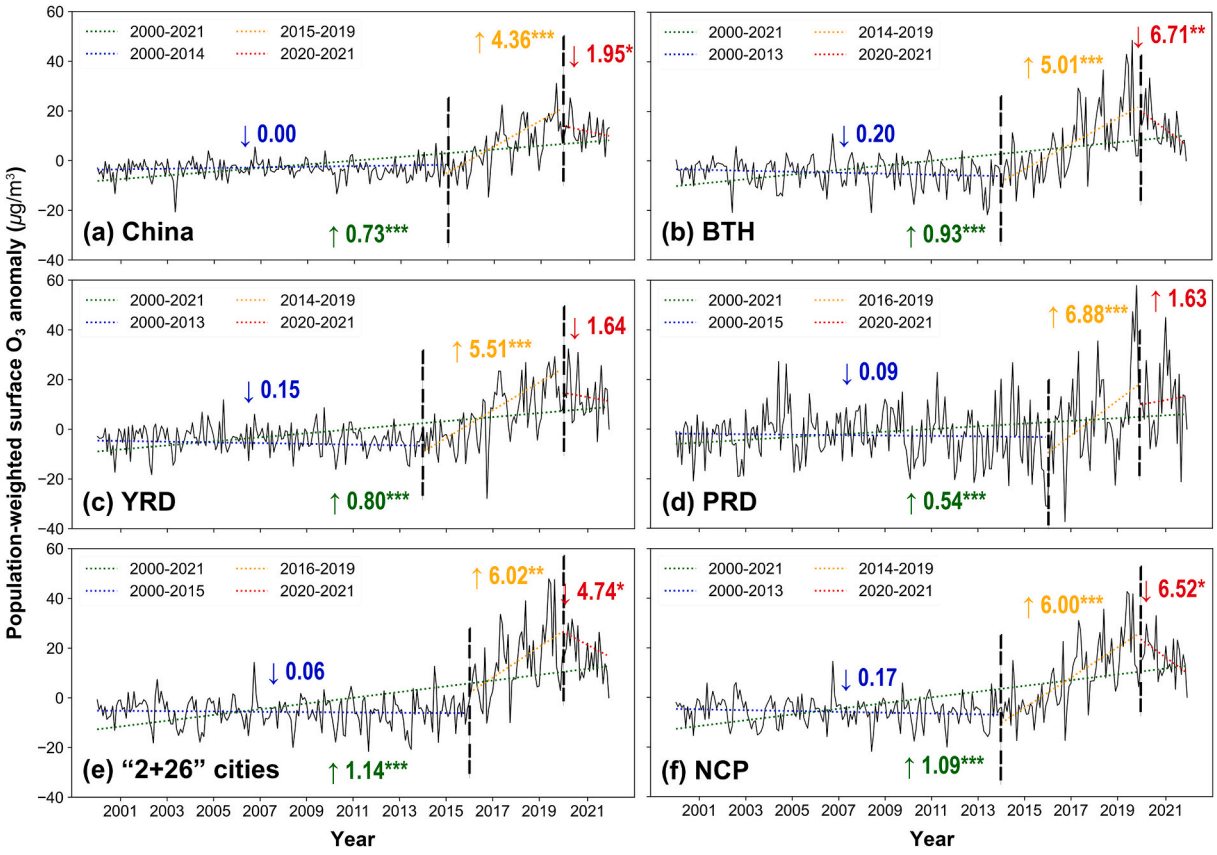

Fig. 5. Time series of monthly population-weighted surface O_3 anomalies and trend lines from 2000 to 2021 across (a) mainland China and (b) the Beijing-Tianjin-Hebei (BTH) region, (c) the Yangtze River Delta (YRD) region, (d) the Pearl River Delta (PRD) region, (e) "2 + 26" cities, and (f) the North China Plain (NCP) region. The green dotted line (value in green) represents the trend (slope of the fitted line from linear regression) over the 22-year period, while other colors (i.e., blue, yellow, and red) represent trends in separate periods determined by the breakpoint detection approach (*: $p < 0.05$, **: $p < 0.01$, ***: $p < 0.001$). (For interpretation of the references to colour in this figure legend, the reader is referred to the web version of this article.)

dataset (Zhao et al., 2022a), specifically in typical urbanized areas (Fig. 6). Over the past two decades 2000–2021, urban areas exhibited a large average relative (absolute) difference, ~12.2 % (12.0 μg/m^3) higher than their rural counterparts in mainland China. Similar distinctive urban-rural differences were also evident at the regional scale, especially in YRD, with an average relative (absolute) difference of 10.0 % (10.4 μg/m^3). Furthermore, the urban-rural contrast changed over time. The national difference increased both before and after 2015, rising from 11.4 μg/m^3 (12.0 %) to 13.8 μg/m^3 (12.8 %). Similarly, in both BTH and PRD regions, the persistent severity of O_3 pollution contributed to a growing disparity in peak-season O_3 concentrations between urban and rural areas, i.e., the relative difference escalated from 6.0 % and 4.9 % before 2015 to 6.5 % and 6.9 % afterwards, respectively. This trend is likely attributed to the positive relationship between the discrepancy in O_3 levels and urbanization (An et al., 2023; Xing et al., 2022), particularly in the PRD, where the urbanization rate from 2016 to 2021 was about six times higher than that from 2000 to 2015 (calculated from the annual urban extents dataset). Increased urbanization likely brought on higher emissions and hotter weather conditions. By contrast, the YRD region had the opposite trend of decreasing urban-rural differences in peak-season O_3 levels. The relative (absolute) difference dropped from 11.9 % (12.0 μg/m^3) during 2000–2015 to 5.0 % (6.0 μg/m^3) during 2016–2021, suggesting that O_3 pollution has been increasingly spreading within the region.

3.3. Population-risk exposure to surface O_3 pollution

3.3.1. Long-term O_3 exposure risk

The 22-year ChinaHighO_3 dataset enables a detailed assessment of health risks due to *long-term* exposure to O_3, guided by WHO's peak-season O_3 standards. During the peak season, severe O_3 pollution reached alarming levels in mainland China from 2000 to 2021 (Fig. 7a). Since 2013, there has been a significant increase in the area exceeding the L-IT1 level (2.57 %/yr, $p < 0.001$) and a concurrent notable rise in the percentage of the population affected (4.73 %/yr, $p < 0.01$). Over the past 22 years, there have been consistent and stable trends in the proportion of areas (days) exceeding the L-IT2 and AQG levels, averaging 45.0 % (99.2 %) and 45.4 % (99.7 %) of the territory (people), respectively. This directly reflects a more pronounced surface O_3 pollution issue in mainland China under the stricter standards. Regional O_3 exposure risks are indeed a notable concern, particularly in BTH (Fig. 7b), e.g., the average proportions of polluted areas exceeding L-IT1, L-IT2, and L-AQG levels are 90.8 %, 93.7 %, and 97.1 %, respectively. On average, over 95 % of the population within the region was exposed to surface O_3 pollution that surpassed these three standards. YRD witnessed the most rapid increase in surpassing the L-IT1 level among all regions post-2013, escalating by 6.58 % per year ($p < 0.01$), while trends under the L-IT2 (L-AQG) level remained relatively stable, with small changes (< 0.03 %/yr) within 94.6 % (94.7 %) each year (Fig. 7c). Meanwhile, there was a significant rise in the percentage of the YRD population experiencing O_3 levels exceeding the L-IT1 level at a rate of 4.13 %/yr ($p < 0.01$) since 2013. Additionally, nearly all the population resided in areas exposed to surface O_3 pollution exceeding the L-IT2 and L-AQG levels (average = 99.5 % and 99.7 %, respectively). In PRD (Fig. 7d), large annual fluctuations were observed at the L-IT1 level, i.e., overall dramatic upward trends of 1.46 %/yr ($p < 0.05$) before 2013 and 5.19 %/yr ($p < 0.05$) after 2013. The extent of O_3-affected areas was more stable, averaging 94.7 % and 95.0 % between 2000 and 2021 for

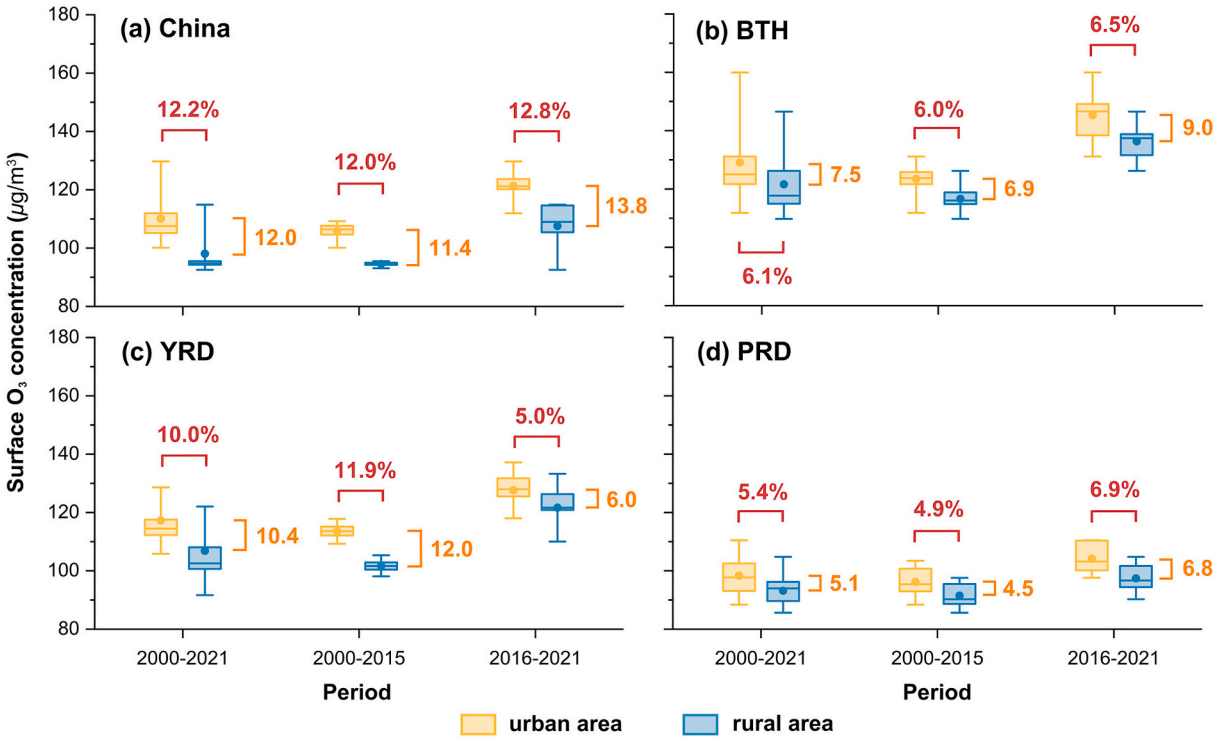

Fig. 6. Comparison of peak-season surface O_3 concentrations between urban (yellow boxes) and rural (blue boxes) areas during different periods (2000–2021, 2000–2015, and 2016–2021) in (a) mainland China and (b-d) three key regions. In each box, the dot signifies the average, and the lower, middle, and upper horizontal lines represent the 25th percentile, median value, and 75th percentile, respectively. Relative (absolute) differences between urban and rural areas are indicated by red (orange) numbers. (For interpretation of the references to colour in this figure legend, the reader is referred to the web version of this article.)

the L-IT2 and L-AQG levels, respectively. Furthermore, the number of people affected by long-term O_3 exposure paralleled the changes in the polluted area for the three recommended standards, underscoring the severity of extreme pollution events in the southern regions of mainland China.

3.3.2. *Short-term O_3 exposure risk*

Our gapless ChinaHighO_3 dataset also enables us to assess the health risks and trends in exposure to *short-term* O_3 pollution at each 1-km^2 grid across mainland China, in accordance with the WHO recommended daily standards (Fig. 8). About 86.9 % of the populated area was exposed to severe O_3 pollution (MDA8 O_3 > S-IT1) for at least one day each year during the 22-year average, with a particularly pronounced impact in the NCP (> 20 %). The percentage of populated areas exposed to pollution showed a notable increase according to both S-IT2 and S-AQG standards, covering almost all inhabited regions in mainland China (~99.8 %) (top panels, Fig. 8). Note that the maximum proportion of polluted days within a 1-km^2 grid is 40 % for the S-IT2 level, reaching up to 60 % for the S-AQG level, notably in the southern regions of China. Temporally, from 2000 to 2021, mainland China experienced a notable rise in the number of days when O_3 pollution in populated areas exceeded recommended levels (bottom panels, Fig. 8), with the most pronounced increase noted in the NCP, followed by southern China. Concerning the S-IT1 level, the magnitudes of the trends across the entirety of eastern China varied little, with ~91.4 % of populated areas displaying a positive trend. Trends for the more stringent S-IT2 and S-AQG criteria show nearly identical patterns, with the proportions of areas of both increasing up to ~97.3 % and many areas experiencing a maximum increase exceeding 2.4 % per year. However, areas that passed the significance test are much smaller in comparison to S-IT1 due to the sustained high proportion of days exceeding S-IT2 and S-AQG criteria throughout the years. Furthermore, over 98 % of 367 Chinese cities experienced ambient O_3 pollution (MDA8 O_3 > 100 μg/m^3) for at least one day since 2017, indicating a persistent and widespread O_3 pollution problem.

Fig. 9 illustrates the annual percentage of areas exceeding the WHO short-term recommended standards for one day, one week, one month, and one quarter of a year in mainland China and different regions for each year during the past two decades. For S-LT1, the occurrence of severe O_3 polluted days in mainland China stayed below one month. However, in recent years, starting from 2017, there has been a continuous expansion in regions experiencing severe O_3 pollution for at least one day (4.63 %/yr, $p = 0.07$) and one week (3.11 %/yr, $p = 0.21$). By contrast, 60 % and 40 % of the BTH region experienced severe O_3 pollution for at least one day and one week, respectively, since 2000. Since 2016, more than half of the region experienced at least one month of severe O_3 pollution. In the YRD, the same annual increase of ~7.2 % ($p < 0.01$) in the percentage of areas where daily MDA8 exceeds 160 μg/m^3 for at least one day and one week was experienced since 2014. This scenario escalated starting in 2017, with over 50 % of the YRD region consistently facing exposure to severe O_3 pollution levels for at least one month. The PRD region had notable interannual variations, with the proportion of area experiencing at least one day (week) exceeding the S-IT1 level, ranging from 22.4 % (1.7 %) in 2000 to 99.0 % (94.1 %) in 2021.

The high daily O_3 pollution risk in mainland China, combined with the close thresholds of the two short-term air quality standards (i.e., S-IT2: daily = 120 μg/m^3, and S-AQG: daily = 100 μg/m^3), results in minimal differences between them. From 2000 to 2021, the average percentage of mainland China's areas exceeding these standards reached 88.4 %, 78.1 %, and 53.4 % for at least one day, one week, and one month of the year, respectively. Additionally, the proportion of areas exceeding these standards for at least 30 days remained below 50 % before 2015 but has since significantly increased (6.59 %/yr, $p < 0.05$). At the regional scale, particularly in BTH, O_3 exposure risks have remained high over time, with equal proportions of 99.3 %, 99.2 %, and

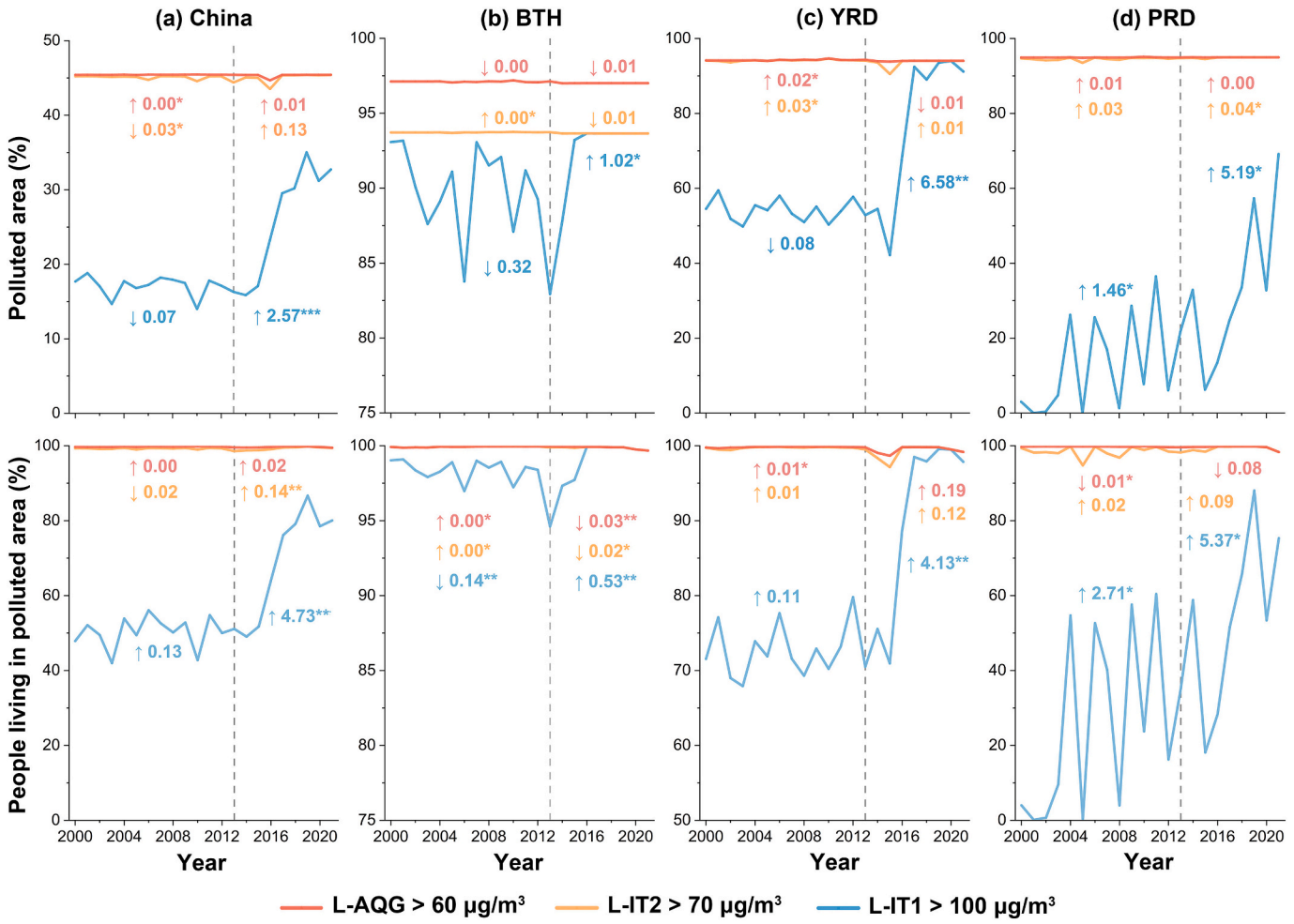

Fig. 7. Percentage of areas exceeding the WHO-recommended long-term air quality standards and percentage of the population experiencing these high pollution levels. The red, orange, and blue lines depict annual peak-season surface O_3 concentrations exceeding 60, 70, and 100 μg/m^3, respectively. The vertical gray line marks the year 2013, with numbers preceding it representing trends from 2000 to 2012 and those following it representing trends from 2013 to 2021. (For interpretation of the references to colour in this figure legend, the reader is referred to the web version of this article.)

94.3 % of the region exceeding the S-AQG and S-IT2 levels for at least one day, one week, and one month, respectively. Since 2016, over 60 % of the BTH region has experienced high O_3 pollution levels (> 120 μg/m^3) for a quarter of the year. The YRD region has shown a significant and substantial upward trend in areas exceeding both the S-AQG and S-IT2 levels, with the same increase in exposure duration [i.e., 0.61 %/yr, 1.09 %/yr, 1.91 %/yr, and 2.50 %/yr, for one day, one week, one month, and one quarter of the year ($p < 0.001$)] over the past two decades. Almost all populated areas in the PRD region exceeded these two standards for at least one day and one week (average = 99.1 % and 98.7 %, respectively) from 2000 to 2021. However, the fluctuations in areal proportions were notably large for at least one month (ranging from 56.7 % to 99.2 %) and especially for a quarter of the year (ranging from 1.1 % to 80.5 %). The year 2019 marked the heaviest O_3 pollution levels, with over 93.6 %, 92.6 %, and 80.5 % of the BTH, YRD, and PRD regions surpassing the S-AQG level for an entire season. This is probably attributable to the sustained rise in precursor emissions from local and transported sources, enhancing O_3 formation via photochemical reactions (Zhang et al., 2023b).

Fig. 10 shows the annual percentage of O_3-polluted days in mainland China and the three typical regions from 2000 to 2021. The national proportion of polluted days was relatively constant with small fluctuations before 2013, but a notable increase occurred after, particularly for the S-AQG (average = 43.8 %) and S-IT2 (average = 16.9 %) levels, with annual growth rates of 3.92 % ($p < 0.001$) and 3.31 % ($p < 0.01$), respectively. Regionally, BTH experienced the highest frequency of O_3 pollution over 22 years, with averages of 9.6 %, 29.2 %, and 41.5 % of days exceeding 160 μg/m^3, 120 μg/m^3, and 100 μg/m^3, respectively. Notably, BTH O_3 pollution underwent a changing point in 2013, with decreasing O_3 before that year, particularly at the S-AQG level (−0.36 %, $p < 0.01$) and increasing O_3 observed for S-IT1 (1.92 %, $p < 0.05$), S-IT2 (1.94 %, $p < 0.01$), and S-AQG (2.30 %, $p < 0.01$) levels. In the YRD, from 2013 to 2021, more significant increases occurred compared to the BTH and PRD regions, as evidenced by a much larger annual rate of 3.16 %/yr ($p < 0.01$) and 3.13 %/yr ($p < 0.01$) for S-AQG and S-IT2 levels, respectively. The interannual oscillation amplitude in the PRD region was relatively large (except for the S-IT1 level), revealing the frequent occurrence of extreme pollution events. There was an overall declining trend until 2016, followed by sharp reversals with significant increases (S-IT2: 2.26 %/yr, $p = 0.15$; S-AQG: 3.55 %/yr, $p < 0.05$).

3.4. Mortality burden attributable to surface O_3 pollution

3.4.1. Long-term O_3 changes and their impact on public health

Studies on the impact of *long-term* O_3 exposure on public health are limited to under a decade due to the lack of long-term surface O_3 data. Here, we first calculated the annual mortality burden exposure to peak-season O_3 pollution from 2000 to 2021 for mainland China and each individual province (Fig. 11). Shandong province recorded the highest accumulated premature deaths during the 22-year period [~164.5 (95

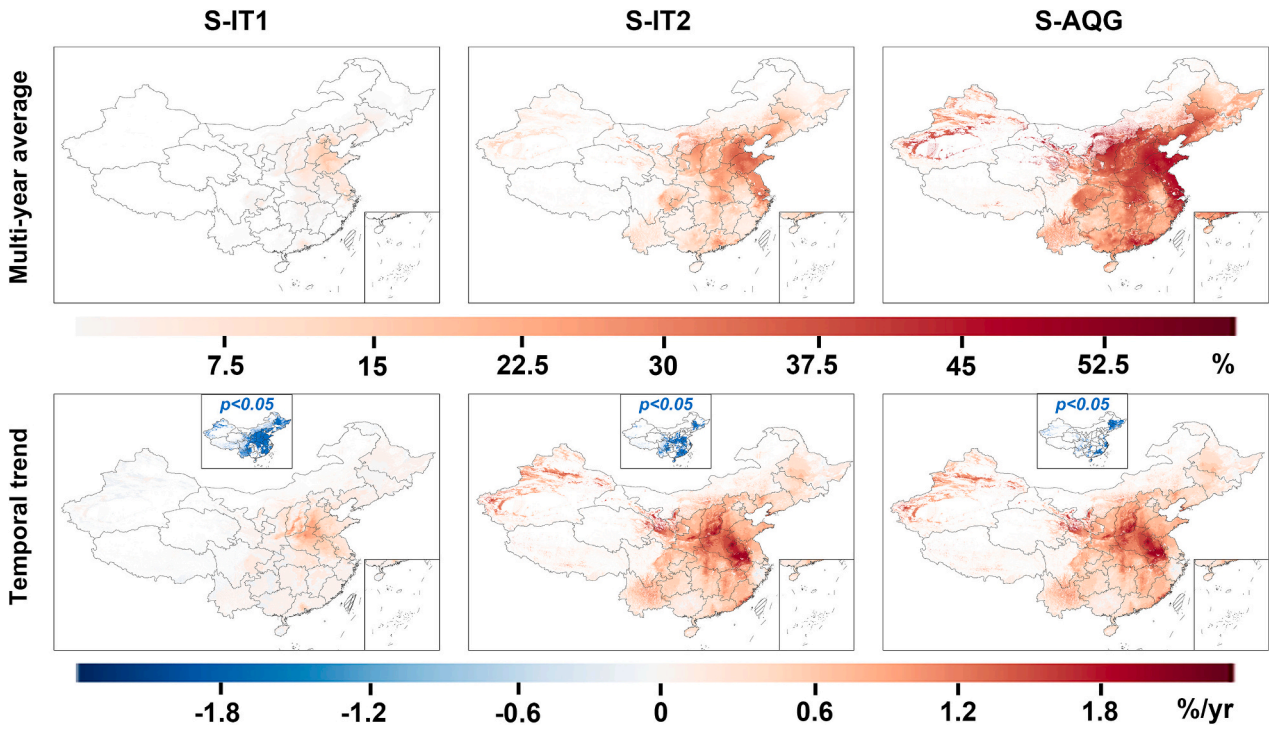

Fig. 8. Annual mean percentage and trend of days exceeding the WHO-recommended short-term air quality standards (S-IT1: daily MDA8 O_3 = 160 μg/m^3, S-IT2: daily MDA8 O_3 = 120 μg/m^3, and S-AQG: daily MDA8 O_3 = 100 μg/m^3) from 2000 to 2021.

% CI: 80.2–231.3) thousand)], followed by Henan [~124.6 (95 % CI: 60.3–176.3) thousand)], Hebei [~117.5 (95 % CI: 57.2–165.2) thousand)], and Jiangsu [~115.2 (95 % CI: 55.7–162.5) thousand)] provinces (Fig. 11a). Sichuan, one of the most populous provinces in mainland China, has been strongly affected by long-term O_3 pollution, leading to an estimated total of 68.0 (95 % CI: 32.5–97.3) thousand deaths over the past two decades. Smaller maps surrounding Fig. 11 show annual changes in fatalities at the provincial level for each year of the last two decades. From 2000 to 2013, there was a slight declining trend in premature deaths in most eastern provinces. However, over the subsequent eight years, a sharp increase occurred, with the year 2019 registering the largest health burden of 93.4 (95 % CI: 45.1–131.4) thousand attributed to O_3 exposure (population-weighted O_3 concentration = 127.3 μg/m^3). Regarding provincial outcomes, Shandong (ranging from 5.1 to 14.2 thousand), Henan (5.0–13.9 thousand), Hebei (4.0–11.1 thousand), and Jiangsu (3.3–9.9 thousand) provinces consistently reported the highest number of lives lost during the past 22 years due to O_3 exposure. By contrast, western provinces (i.e., Xizang, Qinghai, and Yunnan) experienced fewer losses of life. This difference could be linked to more rapid urbanization, as evidenced by the increasing number of urban areas in most Chinese provinces over the past two decades (Fig. S6). This trend is particularly pronounced in the eastern coastal provinces, where growth rates range from 0.13 ‰ to 1.18 ‰ per year, contributing to increased anthropogenic emissions of O_3 precursors. Overall, the increase in surface O_3 concentration has resulted in an uptick in the annual count of premature deaths by 953 (95 % CI: 486–1288, $p < 0.05$) people for the period 2000–2021 (Fig. 11b-c). Additionally, a notable surge has occurred since 2015, particularly between the short period from 2016 to 2019. This increase [13.9 (95 % CI: 5.5–15.8) thousand people per year, $p < 0.01$] corresponds to the most substantial population-weighted O_3 rise (5.9 μg/m^3 per year, $p < 0.01$) nationwide. Since then, the related deaths have steadily decreased to 78.6 (95 % CI: 38.2–111.0) thousand in 2021. Nevertheless, the total burden remains higher than pre-2019 levels. Note that higher temperatures during peak O_3 periods may also influence the associated mortality burden due to the combined health effects of O_3 and heat waves (Xu et al., 2023, 2024a).

3.4.2. *Short-term O_3 changes on public health*

Fig. 12 illustrates the time series of annual accumulated mortality from all days in a year resulting from *short-term* O_3 exposure in mainland China and typical regions, i.e., BTH, YRD, and PRD, from 2000 to 2021, using our daily O_3 concentration dataset. Short-term O_3 exposure has garnered widespread attention, primarily due to the frequent occurrence of extreme pollution events in local regions. Between 2000 and 2013, mainland China witnessed a gradual increase in the number of premature deaths resulting from short-term O_3 exposure, with a rise of 157 people per year (95 % CI: 85–228, $p < 0.01$). Subsequently, the rate of increase sharply accelerated to 2.5 (95 % CI: 1.4–3.7) thousand per year ($p < 0.01$). At the regional scale, all areas have shown a continuous upward trend in short-term O_3-attributed premature deaths since 2000. However, trends in previous years remained relatively stable before 2013, particularly for the BTH region [16 (95 % CI: 11–29) people per year, $p < 0.05$; Fig. 12b], contrary to the PRD region (Fig. 12d), which had the most significant increase, i.e., 44 (95 % CI: 27–55) people per year ($p < 0.001$). The death rate has significantly increased in recent years, especially in the YRD region [483 (95 % CI: 282–654) people per year, $p < 0.01$; Fig. 12c], reaching its peak in 2019, with a total of 5.3 (95 % CI: 2.9–7.7) thousand deaths for the BTH region, 7.9 (95 % CI: 4.2–11.4) thousand deaths for the YRD region, and 1.3 (95 % CI: 0.7–1.8) thousand deaths for the PRD region. Sichuan Basin has also exhibited a significant increasing mortality trend associated with daily O_3 pollution, with an increase of 130 (95 % CI: 63–184) people per year ($p < 0.05$) during 2013–2021, and experienced the highest life loss in 2019 [~2.3 (95 % CI: 1.2–3.1) thousand deaths]. Note that there is a great difference, ~2–3 times for mainland China, in mortality figures calculated from peak-season values compared to results accumulated over all days of the year. This discrepancy arises from the exposure-response functions used. The former is adopted from the worldwide model (GBD 2019 Risk Factors Collaborators, 2020) and may vary

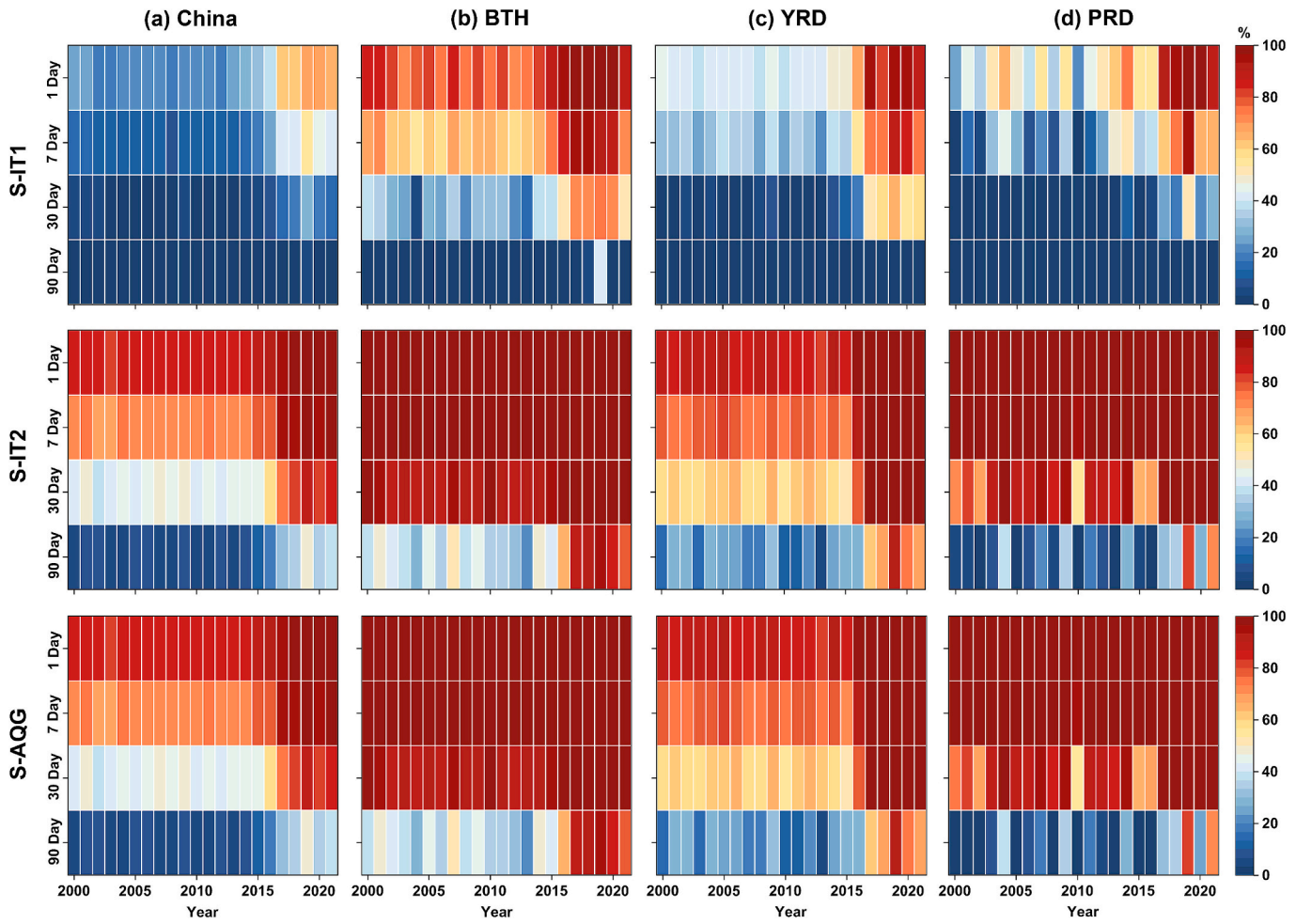

Fig. 9. Percentage of areas of mainland China and different regions (BTH, YRD, and PRD) surpassing the WHO-recommended short-term air quality standards for at least 1 day, 1 week (7 days), 1 month (30 days), and one quarter (90 days) of a year in each year from 2000 to 2021.

greatly across the country and regions (Wei et al., 2023b). The latter uses large cohort data specific to the country.

3.5. Discussion

3.5.1. Impacts of spatial resolution on air quality and health

The spatial resolution of the air quality dataset can influence both the accuracy and effectiveness of assessments of air pollution and mortality burden (Wei et al., 2023b). We thus evaluated differences by comparing surface O_3 polluted levels (Fig. S6) and attributed premature deaths using data at a resolution of 1 km and resampling to a 10-km resolution. On specific days, our 1-km daily O_3 data more accurately identifies important differences in O_3 pollution at the city level, offering more detailed information and showing distinct gradient changes of O_3 pollution within cities. For example, when using Gaussian curves to fit the frequency distributions in the "2 + 26" cities, the 1-km daily O_3 data consistently has higher maximum values in comparison to the coarser-resolution dataset. Peak values can vary greatly, with a relative difference of even up to 17.8 %. This difference is particularly noticeable in key metropolitan clusters, such as the YRD and PRD regions. Additionally, 1-km data also offer a broader spatial coverage around inland rivers, lakes, and land-ocean interfaces. In general, data with the coarse 10-km resolution could underestimate national daily O_3 pollution levels by ~4.8 % compared to 1-km data. Regarding exposure conditions, a small average underestimation of ~1.5 % at the national scale over the long-term perspective when using the coarser 10-km O_3 data is observed. However, with the increasing disparity in population-weighted O_3 concentrations, differences in the number of premature deaths have grown even larger (Fig. 11b): Every 1 % increase in this disparity resulted in a 1.3 % (before 2013) or 3.9 % (after 2013) difference in the number of deaths due to O_3 pollution. In particular, the death-rate trend could be severely underestimated by 13.2 % for long-term surface O_3 exposure. This underestimation becomes even more pronounced for the short-term life loss rate, reaching 19.7 % in mainland China (Fig. 12). This is further evidenced by the substantial underestimations in key urban regions, i.e., YRD (51.4 %), BTH (11.3 %), and PRD (20.5 %), highlighting the importance of higher spatial resolution data for assessing short-term and local (especially urban) air quality and public health.

3.5.2. Comparison with related studies

Many studies are dedicated to estimating surface O_3 concentrations from space. However, few have focused on reconstructing long-term ($\geq$ 5 years) data records in China (Table S2). Previous studies have generally covered a limited time duration, typically around 5–10 years, encountering limitations in terms of coarse spatial resolutions (greater than 5 km or 10 km) or spatial missing values (Chen et al., 2023; Liu et al., 2020; Mu et al., 2023; Wang et al., 2020b; Wei et al., 2022a; Xue et al., 2020; Zhu et al., 2022), restricting their applicability, particularly at urban scales. To overcome these limitations, we made important improvements by incorporating two main predictors—all-sky solar shortwave radiation and surface temperature—from the photochemical reaction perspective of O_3 generation. Our new approach has extended the data records back to 2000 (covering a 22-year period) and enhanced

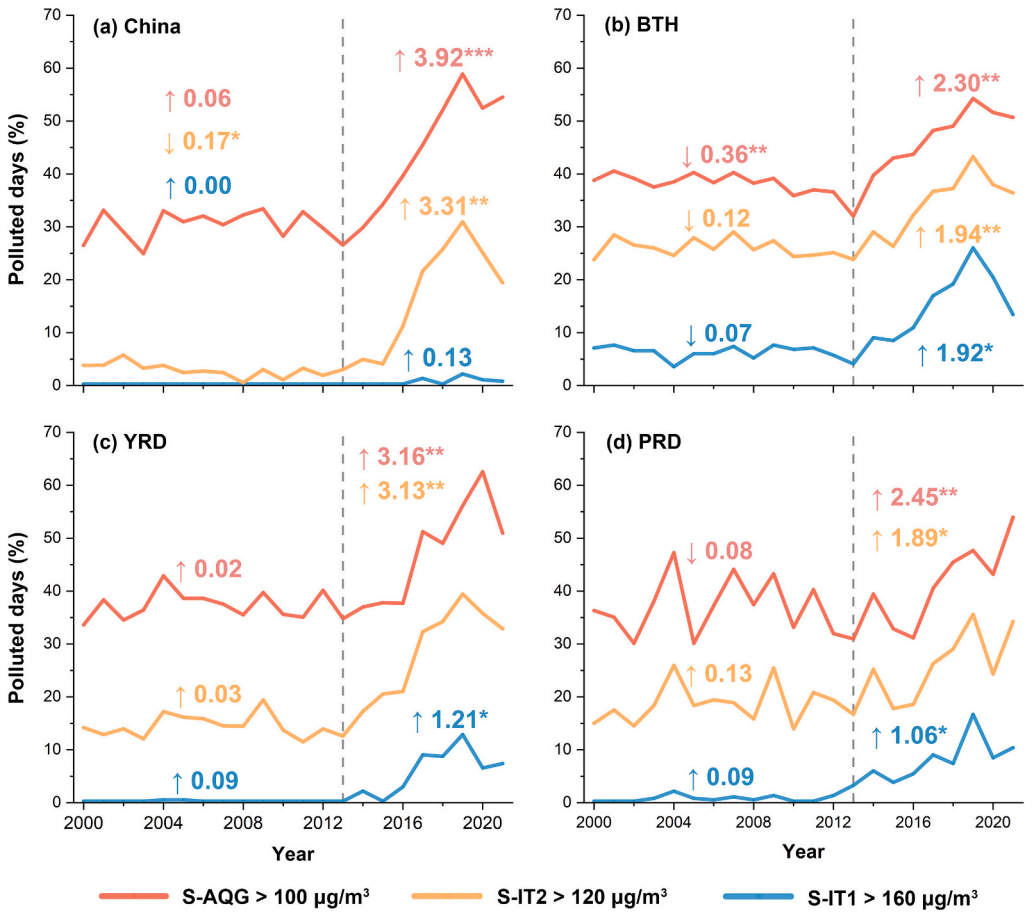

Fig. 10. Time series of percentage of surface-O_3-polluted days exceeding the WHO-recommended short-term S-IT1 (blue lines), S-IT2 (orange lines), and S-AQG (red lines) levels for each year from 2000 to 2021 in (a) mainland China, and the (b) BTH, (c) YRD, and (d) PRD regions. The vertical gray dashed line represents the year 2013, and numbers represent the trends for the periods 2000–2012 and 2013–2021 (*: $p < 0.05$, **: $p < 0.01$, ***: $p < 0.001$). (For interpretation of the references to colour in this figure legend, the reader is referred to the web version of this article.)

the spatial resolution to 1 km, surpassing the resolutions used in other studies by 5–10 times. It also effectively mitigates cloud-contamination challenges, achieving complete 100 % spatial coverage for daily biases. Regarding overall accuracy, our model (CV-R^2 = 0.89, RMSE = 15.77 μg/m^3) outperforms most models developed in most previous studies, such as those using the Nested Air Quality Prediction Modelling System (NAQPMS) atmospheric chemical model (Wang et al., 2020b) and machine- or deep-learning models, including the data-fusion model (CV-R^2 = 0.70, RMSE = 26.00 μg/m^3) (Xue et al., 2020), XGBoost (CV-R^2 = 0.76, RMSE = 21.47 μg/m^3) (Liu et al., 2020), RF (CV-R^2 = 0.87, RMSE = 13.03 μg/m^3) (Zhu et al., 2022), and 3D-CNN (CV-R^2 = 0.88, RMSE = 15.65 μg/m^3) (Mu et al., 2023), improving the CV-R^2 by ~6.8 % and decreasing the RMSE by ~1.9 %. To date, we offer the longest-term coverage (2000 to the present), highest spatial resolution (1 km), and high-quality daily record of surface MDA8 O_3 concentration dataset for mainland China (e.g., ChinaHighO_3).

3.5.3. *Successful applications*

The ChinaHighO_3 dataset has been accessible to the public since December 2020 and successfully applied in various fields, including the environment and climate [e.g., investigating ambient O_3 drivers (Lin et al., 2022), farmland mitigation (He et al., 2022b), air pollution (Cheng et al., 2023; Yang et al., 2024), and extreme weather events (Xia et al., 2022; Xu et al., 2023)], the economy [e.g., assessing economic losses caused by O_3 (Ma et al., 2023)] and the correlation between air quality and high-speed rail (Huang et al., 2023). Notably, a large number of studies in the realm of public health have been conducted, revealing strong associations between long-term and especially short-term exposures to surface O_3 pollution and a variety of human diseases, including lung cancer (Guo et al., 2021), stroke (He et al., 2022a; Li et al., 2023a; Wang et al., 2022a; Xu et al., 2022d; Wu et al., 2022), aigina (Xu et al., 2024), muscle (Zhang et al., 2023a), tuberculosis (Li et al., 2023b), kidney/renal function (Cai et al., 2023b; Li et al., 2022a), diabetes (Hu et al., 2023; Mei et al., 2023; Wang et al., 2022d), death related to dementia (Liu et al., 2022b), cardiovascular disease (Li et al., 2023c; Lv et al., 2023; Xu et al., 2022a; Xu et al., 2022c; Xu et al., 2024a; Tian et al., 2023), chronic ischemic heart disease (Chen et al., 2022a), risk of allosteric load (Xu et al., 2022b), risk of overweight (Han et al., 2023), sleep patterns and quality (Hu et al., 2022; Wang et al., 2022b), metabolic syndrome (Han et al., 2022), sperm quality (Cai et al., 2023a; Zhang et al., 2023c), hepatic enzyme levels (Li et al., 2022b), adults' dislipidemia (Pan et al., 2023), olderly's cognitive impairement (Zhou et al., 2023), hypertension and blood pressure (Niu et al., 2022a), acute myocardial infarction mortalities (Cheng et al., 2023), outpatient visits for anxiety disorders (Xu et al., 2024b), pregnancy birth outcomes (Zhang et al., 2024), as well as attributable mortalities (Liu et al., 2024). These successful applications both confirm and demonstrate the relevance of our dataset in facilitating present and future assessments across various domains. This improved dataset at a 1-km resolution allows for a more in-depth analysis of surface O_3 concentrations at finer scales (urban and suburban) and over an extended temporal period.

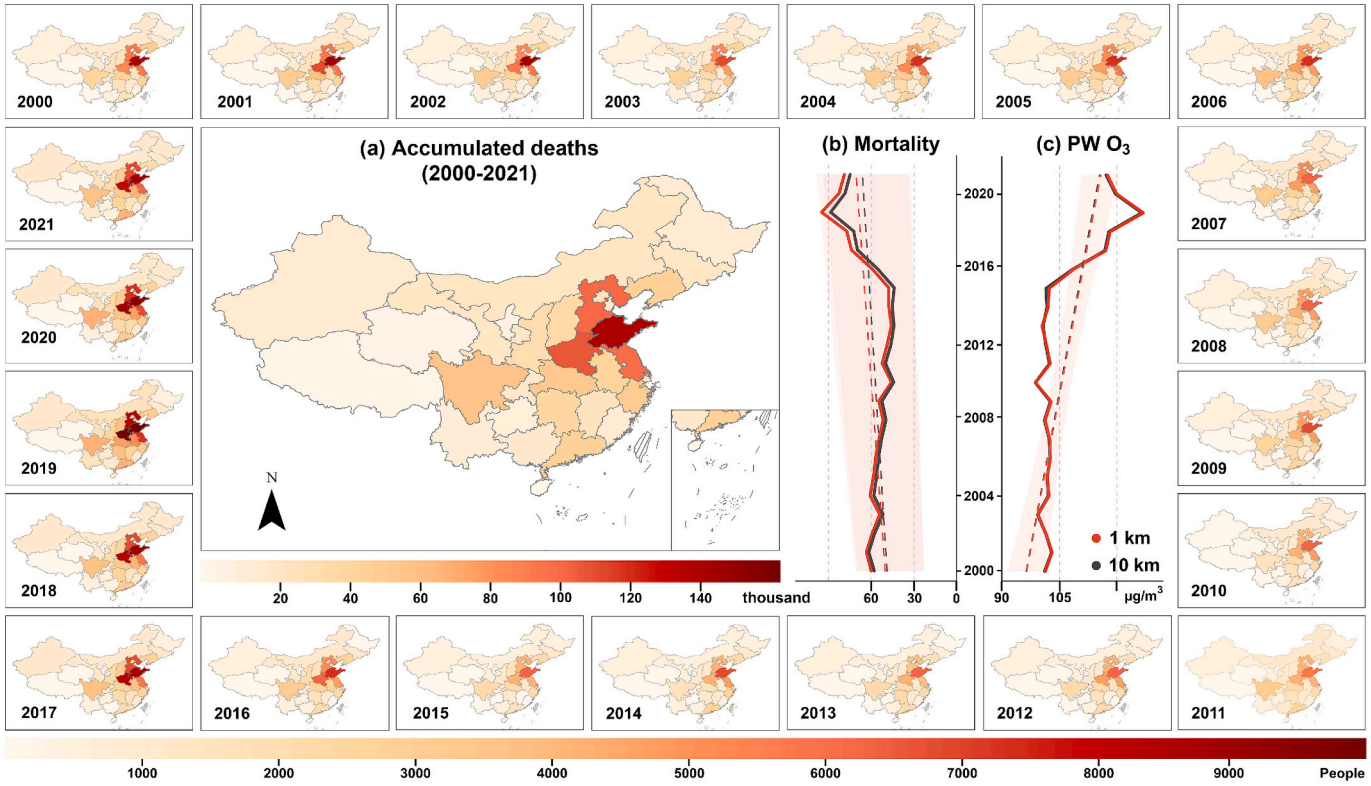

Fig. 11. Spatial distributions of the province-level cumulative number of mortalities attributed to long-term surface O_3 exposure in mainland China (a) for the entire period and each year from 2000 to 2021 (surrounding smaller maps). Panels (b) and (c) show the time series of annual cumulative deaths and population-weighted (PW) surface O_3 concentration from 2000 to 2021. The solid red (black) lines represent the results calculated using the data with a resolution of 1 km (10 km), and the dashed red (black) lines indicate the linear trends, with shaded areas indicating the 95 % confidence interval. (For interpretation of the references to colour in this figure legend, the reader is referred to the web version of this article.)

4. Summary and conclusions

A high spatial resolution and a long time series of ground-level O_3 data are crucial for studying environmental and health-related aspects. Here, we developed the 4D-STDF model to estimate two decades (2000 to the present) of 1-km surface O_3 concentrations covering mainland China. Our approach involved main predictors (satellite-derived 1-km DSR and LST retrievals), integrating national surface O_3 observations, atmospheric reanalysis data, satellite remote sensing products, and an emission inventory. Ten-fold cross-validation results demonstrate high overall accuracy (spatial predictive ability), with sample-based (station-based) CV-R^2, RMSE, and MAE values of 0.89 (0.84), 15.77 (18.74) μg/m^3, and 10.48 (12.36) μg/m^3, respectively. To assess the quality of historical data records, especially before 2013, we conducted independent validations against TOAR measurements, revealing strong correlations at daily (R = 0.80), monthly (R = 0.89), and annual (R = 0.90) levels. Our study outperformed previous studies in terms of time span covered, spatiotemporal resolution, and spatial coverage, also exhibiting superior data quality, with an enhanced CV-R^2 by 6.8 % and a reduced RMSE by 1.9 %. The excellent performance of this product facilitates comprehensive long- and short-term trend analyses of air pollution, particularly the O_3 exposure risk and health burden at finer scales (i.e., at urban and suburban scales) in mainland China.

Leveraging the distinct benefits offered by the ChinaHighO_3 dataset, our study revealed a dynamic and diverse pattern in national, regional, and city-scale surface O_3 levels over the past 22 years. Surface O_3 levels in mainland China remained stable until around 2015, followed by a sharp increase of 4.36 μg/m^3 per year ($p < 0.001$), peaking in 2019 and subsequently declining, especially in the BTH region (−6.71 μg/m^3/yr, $p < 0.01$). In the PRD region, surface O_3 levels have continuously increased since 2016, with a sharp rise during the period 2016–2019 (6.88 μg/m^3/yr, $p < 0.001$). Throughout the peak season, surface O_3 concentrations varied between urban and rural areas, with an average relative difference reaching 12.2 % on a national scale. Moreover, since 2015, mainland China has had a substantial increase in this urban-rural disparity, particularly in the BTH and PRD regions, attributed to the rapid rise in O_3 levels and urbanization rates. Surface O_3 pollution appears to be mostly acceptable under the WHO-recommended long-term (short-term) interim target 1, but 45.0 % (16.9 %) and 45.4 % (43.8 %) of the areas (days) exceeded the interim target 2 and AQG levels in mainland China during the period 2000–2021. Furthermore, since 2013, there has been a substantial growth in the proportion of days exceeding the S-AQG across mainland China and three key urban regions (i.e., BTH, YRD, and PRD), with growth rates of 3.9, 2.3, 3.2, and 2.5 % per year ($p < 0.01$), respectively. Contributing to the increasing severe O_3 exposure risk in mainland China, there were 1308 (95 % CI: 631–1856) thousand mortalities due to long-term O_3 exposure during the total 22-year period, with an annual increasing rate of 953 (95 % CI: 486–1288) deaths per year. The trends in short-term O_3-related mortality in mainland China and typical regions like the BTH and the YRD declined before 2013 but subsequently increased at annual trends of ~2526 (95 % CI: 1373–3672, $p < 0.001$), 298 (95 % CI: 153–409, $p < 0.001$), and 483 (95 % CI: 282–654, $p < 0.001$) thousand per year, respectively. We also determined that when compared with 1-km-resolution data, coarse-resolution (10 km) data could underestimate surface O_3 levels and death-rate trends attributed to long-term (short-term) O_3 exposure by ~1.5 % (4.8 %) and ~13.2 % (19.7 %), respectively. Consequently, our ChinaHighO_3 (1-km daily gapless) dataset is highly useful for understanding long- and short-term O_3 air quality and health issues at medium to small scales, particularly in urban areas.

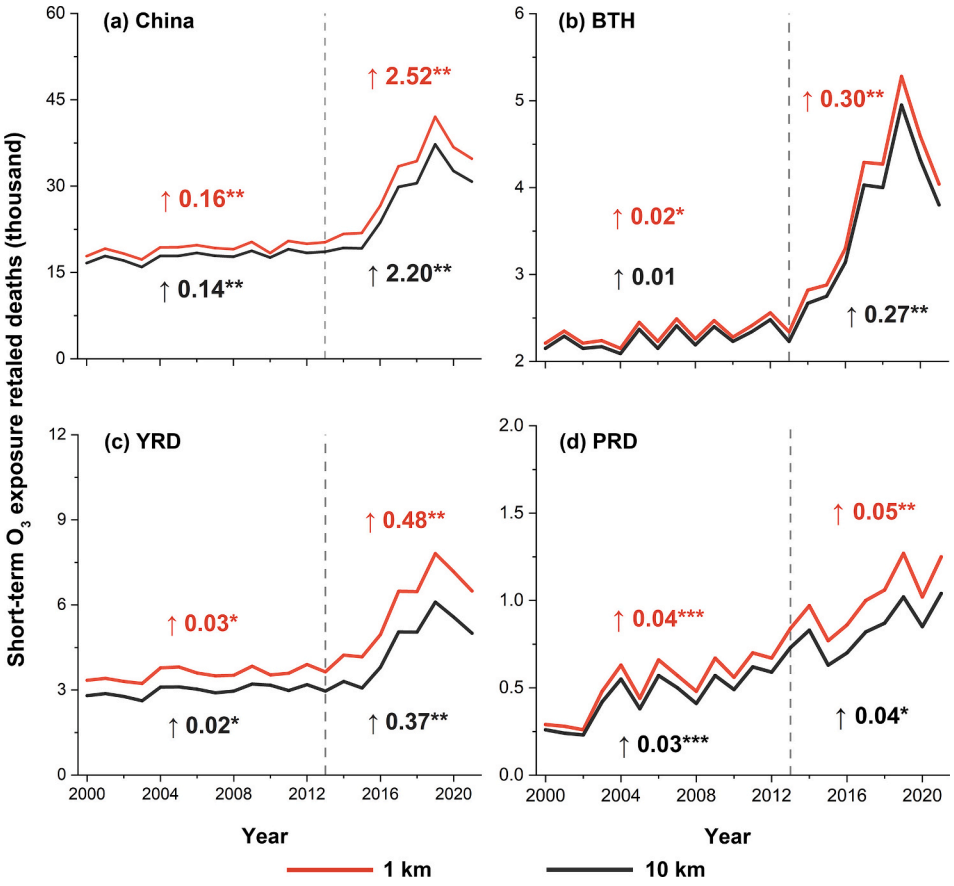

Fig. 12. Time series of annual accumulated mortality from all days in a year attributed to *short-term* surface O_3 exposure across mainland China and other regions (BTH, YRD, and PRD). The red and black lines represent estimated premature deaths using surface O_3 data at 1-km and 10-km resolutions, respectively. The vertical gray dashed line represents the year 2013, and numbers represent the trends for the periods 2000–2012 and 2013–2021. (For interpretation of the references to colour in this figure legend, the reader is referred to the web version of this article.)

CRediT authorship contribution statement

Zeyu Yang: Writing – original draft, Validation, Formal analysis, Data curation. **Zhanqing Li:** Writing – review & editing, Methodology, Investigation, Funding acquisition, Conceptualization. **Fan Cheng:** Data curation. **Qiancheng Lv:** Data curation. **Ke Li:** Writing – review & editing. **Tao Zhang:** Data curation. **Yuyu Zhou:** Data curation. **Bin Zhao:** Data curation. **Wenhao Xue:** Data curation. **Jing Wei:** Writing – review & editing, Methodology, Investigation, Conceptualization.

Declaration of competing interest

The authors declare that they have no conflict of interest.

Data availability

The ChinaHighO_3 dataset is available at https://zenodo.org/doi/10.5281/zenodo.10477125.

Acknowledgments

This work was supported by the National Natural Science Foundation of China (42030606 and 42207541).

Appendix A. Supplementary data

Supplementary data to this article can be found online at https://doi.org/10.1016/j.rse.2024.114459.

References

Adame, J.A., Gutiérrez-Álvarez, I., Cristofanelli, P., Notario, A., Bogeat, J.A., López, A., Gómez, A., Bolívar, J.P., Yela, M., 2022. Surface ozone trends over a 21-year period at El Arenosillo observatory (southwestern Europe). Atmos. Res. 269, 106048. https://doi.org/10.1016/j.atmosres.2022.106048.

An, N., Chen, Y., Zhai, P., Li, J., Wei, Y., 2023. Compound hot and ozone extremes in urban China. Urban Clim. 52, 101689. https://doi.org/10.1016/j.uclim.2023.101689.

Anenberg, S.C., Mohegh, A., Goldberg, D.L., Kerr, G.H., Brauer, M., Burkart, K., Hystad, P., Larkin, A., Wozniak, S., Lamsal, L., 2022. Long-term trends in urban NO_2 concentrations and associated paediatric asthma incidence: estimates from global datasets. Lancet Planetary Health 6, e49–e58. https://doi.org/10.1016/S2542-5196(21)00255-2.

Anghel, A., Papandreou, N., Parnell, T.P., Palma, A.D., Pozidis, H., 2018. Benchmarking and optimization of gradient boosted decision tree algorithms. Arxiv Preprint. https://doi.org/10.48550/arXiv.1809.04559. Arxiv:1809.04559.

Bell, M.L., McDermott, A., Zeger, S.L., Samet, J.M., Dominici, F., 2004. Ozone and short-term mortality in 95 US urban communities, 1987-2000. Jama-J. Am. Med. Assoc. 292, 2372–2378. https://doi.org/10.1001/jama.292.19.2372.

Cai, X., Ni, H., Wang, Q., Dai, T., Wang, L., Song, C., Li, Y., Li, F., Meng, T., Sheng, H., Xiao, L., Xu, T., Yu, X., Zeng, Q., Guo, P., Zhang, X., 2023a. Sperm quality decline associated with gaseous pollutant exposure: evidence from a large cohort multicenter study. J. Hazard. Mater. 460, 132330. https://doi.org/10.1016/j.jhazmat.2023.132330.

Cai, M., Wei, J., Zhang, S., Liu, W., Wang, L., Qian, Z., Lin, H., Liu, E., McMillin, S.E., Cao, Y., Yin, P., 2023b. Short-term air pollution exposure associated with death from kidney diseases: a nationwide time-stratified case-crossover study in China from 2015 to 2019. BMC Med. 21, 32. https://doi.org/10.1186/s12916-023-02734-9.

Chen, G., Chen, J., Dong, G., Yang, B., Liu, Y., Lu, T., Yu, P., Guo, Y., Li, S., 2021. Improving satellite-based estimation of surface ozone across China during 2008–2019 using iterative random forest model and high-resolution grid meteorological data. Sustain. Cities Soc. 69, 102807. https://doi.org/10.1016/j.scs.2021.102807.

Chen, Q., Chen, Q., Wang, Q., Xu, R., Liu, T., Liu, Y., Ding, Z., Sun, H., 2022a. Particulate matter and ozone might trigger deaths from chronic ischemic heart disease. Ecotox. Environ. Safe. 242, 113931. https://doi.org/10.1016/j.ecoenv.2022.113931.

Chen, Y., Zhou, Y., Ciren, Nixia, Zhang, H., Wang, C., Deji, Gesang, Wang, X., 2022b. Spatiotemporal variations of surface ozone and its influencing factors across Tibet: a Geodetector-based study. Sci. Total Environ. 813, 152651. https://doi.org/10.1016/j.scitotenv.2021.152651.

Chen, B., Wang, Y., Huang, J., Zhao, L., Chen, R., Song, Z., Hu, J., 2023. Estimation of near-surface ozone concentration and analysis of main weather situation in China based on machine learning model and Himawari-8 TOAR data. Sci. Total Environ. 864, 160928. https://doi.org/10.1016/j.scitotenv.2022.160928.

Cheng, J., Zheng, H., Wei, J., Huang, C., Ho, H.C., Sun, S., Phung, D., Kim, H., Wang, X., Bai, Z., Hossain, M.Z., Tong, S., Su, H., Xu, Z., 2023. Short-term residential exposure to air pollution and risk of acute myocardial infarction deaths at home in China. Environ. Sci. Pollut. R. 30, 76881–76890. https://doi.org/10.1007/s11356-023-27813-5.

Czechowski, P.O., Romanowska, A., Czermański, E., Oniszczuk-Jastrząbek, A., Wanagos, M., 2023. An attempt to determine the relationship between air pollution and the real estate market in 2010–2020 in Gdańsk using GLM and GRM statistical models. Sustainability 15 (3), 2471. https://doi.org/10.3390/su15032471.

GBD 2019 Risk Factors Collaborators, 2020. Global burden of 87 risk factors in 204 countries and territories, 1990–2019: a systematic analysis for the Global Burden of Disease Study 2019. Lancet 396, 1223–1249. https://doi.org/10.1016/S0140-6736(20)30752-2.

Guan, Y., Xiao, Y., Wang, Y., Zhang, N., Chu, C., 2021. Assessing the health impacts attributable to $PM_{2.5}$ and ozone pollution in 338 Chinese cities from 2015 to 2020. Environ. Pollut. 287, 117623. https://doi.org/10.1016/j.envpol.2021.117623.

Guo, H., Liu, J., Wei, J., 2021. Ambient ozone, PM_1 and female lung Cancer incidence in 436 Chinese counties. J. Environ. Res. Public Health 18 (19), 10386. https://doi.org/10.3390/ijerph181910386.

Han, S., Zhang, F., Yu, H., Wei, J., Xue, L., Duan, Z., Niu, Z., 2022. Systemic inflammation accelerates the adverse effects of air pollution on metabolic syndrome: findings from the China health and retirement longitudinal study (CHARLS). Environ. Res. 215, 114340. https://doi.org/10.1016/j.envres.2022.114340.

Han, W., Xu, Z., Hu, X., Cao, R., Wang, Y., Jin, J., Wang, J., Yang, T., Zeng, Q., Huang, J., Li, G., 2023. Air pollution, greenness and risk of overweight among middle-aged and older adults: a cohort study in China. Environ. Res. 216, 114372. https://doi.org/10.1016/j.envres.2022.114372.

Hashim, B.M., Al-Naseri, S.K., Al-Maliki, A., Al-Ansari, N., 2021. Impact of COVID-19 lockdown on NO_2, O_3, $PM_{2.5}$ and PM_{10} concentrations and assessing air quality changes in Baghdad, Iraq. Sci. Total Environ. 754, 141978. https://doi.org/10.1016/j.scitotenv.2020.141978.

He, F., Wei, J., Dong, Y., Liu, C., Zhao, K., Peng, W., Lu, Z., Zhang, B., Xue, F., Guo, X., Jia, X., 2022a. Associations of ambient temperature with mortality for ischemic and hemorrhagic stroke and the modification effects of greenness in Shandong Province, China. Sci. Total Environ. 851, 158046. https://doi.org/10.1016/j.scitotenv.2022.158046.

He, L., Wei, J., Wang, Y., Shang, Q., Liu, J., Yin, Y., Frankenberg, C., Jiang, J.H., Li, Z., Yung, Y.L., 2022b. Marked impacts of pollution mitigation on crop yields in China. Earth's Future 10. https://doi.org/10.1029/2022EF002936 e2022EF002936.

Hu, K., Li, W., Zhang, Y., Chen, H., Bai, C., Yang, Z., Lorenz, T., Liu, K., Shirai, K., Song, J., Zhao, Q., Zhao, Y., Zhang, J.J., Wei, J., Pan, J., Qi, J., Ye, T., Zeng, Y., Yao, Y., 2022. Association between outdoor artificial light at night and sleep duration among older adults in China: a cross-sectional study. Environ. Res. 212, 113343. https://doi.org/10.1016/j.envres.2022.113343.

Hu, K., Zhang, Z., Li, Y., Wang, S., Ye, T., Song, J., Zhang, Y., Wei, J., Cheng, J., Shen, Y., Pan, J., Fu, J., Qi, J., Guo, Y., Zeng, Y., Yao, Y., 2023. Urban overall and visible greenness and diabetes among older adults in China. Landsc. Urban Plan. 240, 104881. https://doi.org/10.1016/j.landurbplan.2023.104881.

Huang, Y., Ma, L., Cao, J., 2023. Exploring spatial heterogeneity in the high-speed rail impact on air quality. J. Transp. Geogr. 106, 103498. https://doi.org/10.1016/j.jtrangeo.2022.103498.

Lelieveld, J., Dentener, F.J., 2000. What controls tropospheric ozone? J. Geophys. Res. Atmos. 105, 3531–3551. https://doi.org/10.1029/1999JD901011.

Li, M., Wang, T., Shu, L., Qu, Y., Xie, M., Liu, J., Wu, H., Kalsoom, U., 2021. Rising surface ozone in China from 2013 to 2017: a response to the recent atmospheric warming or pollutant controls? Atmos. Environ. 246, 118130. https://doi.org/10.1016/j.atmosenv.2020.118130.

Li, S., Meng, Q., Laba, C., Guan, H., Wang, Z., Pan, Y., Wei, J., Xu, H., Zeng, C., Wang, X., Jiang, M., Lu, R., Guo, B., Zhao, X., 2022a. Associations between long-term exposure to ambient air pollution and renal function in Southwest China: the China multi-ethnic cohort (CMEC) study. Ecotox. Environ. Safe. 242, 113851. https://doi.org/10.1016/j.ecoenv.2022.113851.

Li, S., Wang, S., Wu, Q., Zhang, Y., Ouyang, D., Zheng, H., Han, L., Qiu, X., Wen, Y., Liu, M., Jiang, Y., Yin, D., Liu, K., Zhao, B., Zhang, S., Wu, Y., Hao, J., 2023. Emission trends of air pollutants and CO_2 in China from 2005 to 2021. Earth Syst. Sci. Data 15, 2279–2294. https://doi.org/10.5194/essd-15-2279-2023.

Li, Y., Yuan, X., Wei, J., Sun, Y., Ni, W., Zhang, H., Zhang, Y., Wang, R., Xu, R., Liu, T., Yang, C., Chen, G., Xu, J., Liu, Y., 2022b. Long-term exposure to ambient air pollution and serum liver enzymes in older adults: a population-based longitudinal study. Ann. Epidemiol. 74, 1–7. https://doi.org/10.1016/j.annepidem.2022.05.011.

Li, M., Edgell, R.C., Wei, J., Li, H., Qian, Z.M., Feng, J., Tian, F., Wang, X., Xin, Q., Cai, M., Lin, H., 2023a. Air pollution and stroke hospitalization in the Beibu gulf region of China: a case-crossover analysis. Ecotox. Environ. Safe. 255, 114814. https://doi.org/10.1016/j.ecoenv.2023.114814.

Li, J., Luan, Q., Li, B., Dharmage, S.C., Heinrich, J., Bloom, M.S., Knibbs, L.D., Popovic, I., Li, L., Zhong, X., Xu, A., He, C., Liu, K., Liu, X., Chen, G., Xiang, M., Yu, Y., Guo, Y., Dong, G., Zou, X., Yang, B., 2023b. Outdoor environmental exposome and the burden of tuberculosis: findings from nearly two million adults in northwestern China. J. Hazard. Mater. 459, 132222. https://doi.org/10.1016/j.jhazmat.2023.132222.

Li, J., Tang, W., Li, S., He, C., Dai, Y., Feng, S., Zeng, C., Yang, T., Meng, Q., Meng, J., Pan, Y., Deji, S., Zhang, J., Xie, L., Guo, B., Lin, H., Zhao, X., 2023c. Ambient $PM_{2.5}$ and its components associated with 10-year atherosclerotic cardiovascular disease risk in Chinese adults. Ecotox. Environ. Safe. 263, 115371. https://doi.org/10.1016/j.ecoenv.2023.115371.

Lin, W., Zhu, T., Song, Y., Zou, H., Tang, M., Tang, X., Hu, J., 2008. Photolysis of surface O3 and production potential of OH radicals in the atmosphere over the Tibetan plateau. J. Geophys. Res. Atmos. 113. https://doi.org/10.1029/2007JD008831.

Lin, H., Zhu, J., Jiang, P., Cai, Z., Yang, X., Yang, X., Zhou, Z., Wei, J., 2022. Assessing drivers of coordinated control of ozone and fine particulate pollution: evidence from Yangtze River Delta in China. Environ. Impact Asses. 96, 106840. https://doi.org/10.1016/j.eiar.2022.106840.

Liu, Y., Pan, J., Zhang, H., Shi, C., Li, G., Peng, Z., Ma, J., Zhou, Y., Zhang, L., 2019a. Short-term exposure to ambient air pollution and asthma mortality. Am. J. Resp. Crit. Care 200, 24–32. https://doi.org/10.1164/rccm.201810-1823OC.

Liu, X., Tian, Y., Lei, X., Liu, M., Wen, X., Huang, H., Wang, H., 2019b. Deep forest based intelligent fault diagnosis of hydraulic turbine. J. Mech. Sci. Technol. 33, 2049–2058. https://doi.org/10.1007/s12206-019-0408-9.

Liu, R., Ma, Z., Liu, Y., Shao, Y., Zhao, W., Bi, J., 2020. Spatiotemporal distributions of surface ozone levels in China from 2005 to 2017: a machine learning approach. Environ. Int. 142, 105823. https://doi.org/10.1016/j.envint.2020.105823.

Liu, J., Yin, H., Tang, X., Zhu, T., Zhang, Q., Liu, Z., Tang, X., Yi, H., 2021. Transition in air pollution, disease burden and health cost in China: a comparative study of long-term and short-term exposure. Environ. Pollut. 277, 116770. https://doi.org/10.1016/j.envpol.2021.116770.

Liu, W., Hegglin, M.I., Checa-Garcia, R., Li, S., Gillett, N.P., Lyu, K., Zhang, X., Swart, N. C., 2022a. Stratospheric ozone depletion and tropospheric ozone increases drive Southern Ocean interior warming. Nat. Clim. Chang. 12, 365–372. https://doi.org/10.1038/s41558-022-01320-w.

Liu, T., Zhou, Y., Wei, J., Chen, Q., Xu, R., Pan, J., Lu, W., Wang, Y., Fan, Z., Li, Y., Xu, L., Cui, X., Shi, C., Zhang, L., Chen, X., Bao, W., Sun, H., Liu, Y., 2022b. Association between short-term exposure to ambient air pollution and dementia mortality in Chinese adults. Sci. Total Environ. 849, 157860. https://doi.org/10.1016/j.scitotenv.2022.157860.

Liu, S., Li, X., Wei, J., Shu, L., Jin, J., Fu, T., Yang, X., Zhu, L., 2024. Short-term exposure to fine particulate matter and ozone: source impacts and attributable mortalities. Environ. Sci. Technol. 58, 11256–11267. https://doi.org/10.1021/acs.est.4c00339.

Lu, X., Zhang, S., Xing, J., Wang, Y., Chen, W., Ding, D., Wu, Y., Wang, S., Duan, L., Hao, J., 2020a. Progress of air pollution control in China and its challenges and opportunities in the ecological civilization era. Engineering-Prc 6, 1423–1431. https://doi.org/10.1016/j.eng.2020.03.014.

Lu, X., Zhang, L., Wang, X., Gao, M., Li, K., Zhang, Y., Yue, X., Zhang, Y., 2020b. Rapid increases in warm-season surface ozone and resulting health impact in China since 2013. Environ Sci Tech Let 7, 240–247. https://doi.org/10.1021/acs.estlett.0c00171.

Lv, S., Shi, Y., Xue, Y., Hu, Y., Hu, M., Li, S., Xie, W., Li, Y., Ouyang, Y., Li, Z., Liu, M., Wei, J., Guo, X., Liu, X., 2023. Long-term effects of particulate matter on incident cardiovascular diseases in middle-aged and elder adults: the CHARLS cohort study. Ecotox. Environ. Safe. 262, 115181. https://doi.org/10.1016/j.ecoenv.2023.115181.

Lyu, X., Li, K., Guo, H., Morawska, L., Zhou, B., Zeren, Y., Jiang, F., Chen, C., Goldstein, A.H., Xu, X., Wang, T., Lu, X., Zhu, T., Querol, X., Chatani, S., Latif, M.T., Schuch, D., Sinha, V., Kumar, P., Mullins, B., Seguel, R., Shao, M., Xue, L., Wang, N., Chen, J., Gao, J., Chai, F., Simpson, I., Sinha, B., Blake, D.R., 2023. A synergistic ozone-climate control to address emerging ozone pollution challenges. One Earth 6, 964–977. https://doi.org/10.1016/j.oneear.2023.07.004.

Ma, Y., Zhang, Y., Wang, W., Qin, P., Li, H., Jiao, H., Wei, J., 2023. Estimation of health risk and economic loss attributable to $PM_{2.5}$ and O_3 pollution in Jilin Province, China. Sci Rep-Uk 13, 17717. https://doi.org/10.1038/s41598-023-45062-x.

Maji, K.J., Ye, W., Arora, M., Nagendra, S.M.S., 2019. Ozone pollution in Chinese cities: assessment of seasonal variation, health effects and economic burden. Environ. Pollut. 247, 792–801. https://doi.org/10.1016/j.envpol.2019.01.049.

McConnell, R., Berhane, K., Gilliland, F., London, S.J., Islam, T., Gauderman, W.J., Avol, E., Margolis, H.G., Peters, J.M., 2002. Asthma in exercising children exposed to ozone: a cohort study. Lancet 359, 386–391. https://doi.org/10.1016/S0140-6736(02)07597-9.

MEE, 2018. Ministry of Ecology and Environment (MEE), 2018. Revision of the Ambien air Quality Standards (GB 3095–2012) (in Chinese). https://english.mee.gov.cn/Resources/standards/Air_Environment/quality_standard1/201605/t20160511_337502.shtmlh.

Mei, Y., Li, A., Zhao, J., Zhou, Q., Zhao, M., Xu, J., Li, R., Li, Y., Li, K., Ge, X., Guo, C., Wei, Y., Xu, Q., 2023. Association of long-term air pollution exposure with the risk of prediabetes and diabetes: systematic perspective from inflammatory mechanisms, glucose homeostasis pathway to preventive strategies. Environ. Res. 216, 114472. https://doi.org/10.1016/j.envres.2022.114472.

Meng, X., Wang, W., Shi, S., Zhu, S., Wang, P., Chen, R., Xiao, Q., Xue, T., Geng, G., Zhang, Q., Kan, H., Zhang, H., 2022. Evaluating the spatiotemporal ozone characteristics with high-resolution predictions in mainland China, 2013–2019. Environ. Pollut. 299, 118865. https://doi.org/10.1016/j.envpol.2022.118865.

Mousavinezhad, S., Choi, Y., Pouyaei, A., Ghahremanloo, M., Nelson, D.L., 2021. A comprehensive investigation of surface ozone pollution in China, 2015–2019: separating the contributions from meteorology and precursor emissions. Atmos. Res. 257, 105599. https://doi.org/10.1016/j.atmosres.2021.105599.

Mu, X., Wang, S., Jiang, P., Wang, B., Wu, Y., Zhu, L., 2023. Full-coverage spatiotemporal estimation of surface ozone over China based on a high-efficiency deep learning model. Int J. Appl Earth Obs 118, 103284. https://doi.org/10.1016/j.jag.2023.103284.

Niu, Z., Duan, Z., Wei, J., Wang, F., Han, D., Zhang, K., Jing, Y., Wen, W., Qin, W., Yang, X., 2022a. Associations of long-term exposure to ambient ozone with hypertension, blood pressure, and the mediation effects of body mass index: a national cross-sectional study of middle-aged and older adults in China. Ecotox. Environ. Safe. 242, 113901. https://doi.org/10.1016/j.ecoenv.2022.113901.

Niu, Y., Zhou, Y., Chen, R., Yin, P., Meng, X., Wang, W., Liu, C., Ji, J.S., Qiu, Y., Kan, H., Zhou, M., 2022b. Long-term exposure to ozone and cardiovascular mortality in China: a nationwide cohort study. Lancet Planetary Health 6, e496–e503. https://doi.org/10.1016/S2542-5196(22)00093-6.

Oberkampf, W.L., Roy, C.J., 2010. Verification and Validation in Scientific Computing. Cambridge University Press. Model Accuracy Assessment, England, Cambridge, pp. 469–554. https://doi.org/10.1017/CBO9780511760396.017.

Orellano, P., Reynoso, J., Quaranta, N., Bardach, A., Ciapponi, A., 2020. Short-term exposure to particulate matter (PM_{10} and $PM_{2.5}$), nitrogen dioxide (NO_2), and ozone (O_3) and all-cause and cause-specific mortality: systematic review and meta-analysis. Environ. Int. 142, 105876. https://doi.org/10.1016/j.envint.2020.105876.

Pan, X., Hong, F., Li, S., Wu, J., Xu, H., Yang, S., Chen, K., Baima, K., Nima, Q., Meng, Q., Xia, J., Xu, J., Guo, B., Lin, H., Xie, L., Zhang, J., Zhao, X., 2023. Long-term exposure to ambient $PM_{2.5}$ constituents is associated with dyslipidemia in Chinese adults. Ecotox. Environ. Safe. 263, 115384. https://doi.org/10.1016/j.ecoenv.2023.115384.

Ren, J., Guo, F., Xie, S., 2022. Diagnosing ozone–NO_x–VOC sensitivity and revealing causes of ozone increases in China based on 2013–2021 satellite retrievals. Atmos. Chem. Phys. 22, 15035–15047. https://doi.org/10.5194/acp-22-15035-2022.

Sadiq, M., Tai, A.P.K., Lombardozzi, D., Val Martin, M., 2017. Effects of ozone–vegetation coupling on surface ozone air quality via biogeochemical and meteorological feedbacks. Atmos. Chem. Phys. 17, 3055–3066. https://doi.org/10.5194/acp-17-3055-2017.

Schlink, U., Herbarth, O., Richter, M., Dorling, S., Nunnari, G., Cawley, G., Pelikan, E., 2006. Statistical models to assess the health effects and to forecast ground-level ozone. Environ. Model. Softw. 21, 547–558. https://doi.org/10.1016/j.envsoft.2004.12.002.

Soares, A.R., Silva, C., 2022. Review of ground-level ozone impact in respiratory health deterioration for the past two decades. Atmosphere. 13 (3), 434. https://doi.org/10.3390/atmos13030434.

Taylan, O., 2017. Modelling and analysis of ozone concentration by artificial intelligent techniques for estimating air quality. Atmos. Environ. 150, 356–365. https://doi.org/10.1016/j.atmosenv.2016.11.030.

Tian, Y., Wu, J., Wu, Y., Wang, M., Wang, S., Yang, R., Wang, X., Wang, J., Yu, H., Li, D., Wu, T., Wei, J., Hu, Y., 2023. Short-term exposure to reduced specific-size ambient particulate matter increase the risk of cause-specific cardiovascular disease: a national-wide evidence from hospital admissions. Ecotox. Environ. Safe. 263, 115327. https://doi.org/10.1016/j.ecoenv.2023.115327.

Turner, M.C., Jerrett, M., Pope, C.A., Krewski, D., Gapstur, S.M., Diver, W.R., Beckerman, B.S., Marshall, J.D., Su, J., Crouse, D.L., Burnett, R.T., 2015. Long-term ozone exposure and mortality in a large prospective study. Am. J. Resp. Crit. Care 193, 1134–1142. https://doi.org/10.1164/rccm.201508-1633OC.

Wang, D., Liang, S., Zhang, Y., Gao, X., Brown, M.G.L., Jia, A., 2020a. A new set of MODIS land products (MCD18): downward shortwave radiation and photosynthetically active radiation. Remote Sens. 12, 168. https://doi.org/10.3390/rs12010168.

Wang, Y., Wild, O., Chen, X., Wu, Q., Gao, M., Chen, H., Qi, Y., Wang, Z., 2020b. Health impacts of long-term ozone exposure in China over 2013–2017. Environ. Int. 144, 106030. https://doi.org/10.1016/j.envint.2020.106030.

Wang, F., Qiu, X., Cao, J., Peng, L., Zhang, N., Yan, Y., Li, R., 2021. Policy-driven changes in the health risk of $PM_{2.5}$ and O_3 exposure in China during 2013–2018. Sci. Total Environ. 757, 143775. https://doi.org/10.1016/j.scitotenv.2020.143775.

Wang, R., Xu, R., Wei, J., Liu, T., Ye, Y., Li, Y., Lin, Q., Zhou, Y., Huang, S., Lv, Z., Tian, Q., Liu, Y., 2022a. Short-term exposure to ambient air pollution and hospital admissions for sequelae of stroke in Chinese older adults. Geohealth 6. https://doi.org/10.1029/2022GH000700 e2022GH000700.

Wang, L., Zhang, J., Wei, J., Zong, J., Lu, C., Du, Y., Wang, Q., 2022b. Association of ambient air pollution exposure and its variability with subjective sleep quality in China: a multilevel modeling analysis. Environ. Pollut. 312, 120020. https://doi.org/10.1016/j.envpol.2022.120020.

Wang, Y., Wang, K., Cheng, W., Zhang, Y., 2022c. Global burden of chronic obstructive pulmonary disease attributable to ambient ozone in 204 countries and territories during 1990–2019. Environ. Sci. Pollut. R. 29, 9293–9305. https://doi.org/10.1007/s11356-021-16233-y.

Wang, Y., Cao, R., Xu, Z., Jin, J., Wang, J., Yang, T., Wei, J., Huang, J., Li, G., 2022d. Long-term exposure to ozone and diabetes incidence: a longitudinal cohort study in China. Sci. Total Environ. 816, 151634. https://doi.org/10.1016/j.scitotenv.2021.151634.

Wang, L., Liu, B., Li, R., Chen, X., Liu, L., Tang, X., Liu, J., Liao, Z., Xin, J., Wang, Y., Hu, B., 2023a. Prediction of daily $PM_{2.5}$ and ozone based on high-density weather stations in China: nonlinear effects of meteorology, human and ecosystem health risks. Atmos. Res. 293, 106889. https://doi.org/10.1016/j.atmosres.2023.106889.

Wang, Y., Zhao, Y., Liu, Y., Jiang, Y., Zheng, B., Xing, J., Liu, Y., Wang, S., Nielsen, C.P., 2023b. Sustained emission reductions have restrained the ozone pollution over China. Nat. Geosci. 16, 967–974. https://doi.org/10.1038/s41561-023-01284-2.

Wei, J., Peng, Y., Mahmood, R., Sun, L., Guo, J., 2019. Intercomparison in spatial distributions and temporal trends derived from multi-source satellite aerosol products. Atmos. Chem. Phys. 19, 7183–7207. https://doi.org/10.5194/acp-19-7183-2019.

Wei, J., Li, Z., Lyapustin, A., Sun, L., Peng, Y., Xue, W., Su, T., Cribb, M., 2021. Reconstructing 1-km-resolution high-quality $PM_{2.5}$ data records from 2000 to 2018 in China: spatiotemporal variations and policy implications. Remote Sens. Environ. 252, 112136. https://doi.org/10.1016/j.rse.2020.112136.

Wei, J., Li, Z., Li, K., Dickerson, R.R., Pinker, R.T., Wang, J., Liu, X., Sun, L., Xue, W., Cribb, M., 2022a. Full-coverage mapping and spatiotemporal variations of ground-level ozone (O_3) pollution from 2013 to 2020 across China. Remote Sens. Environ. 270, 112775. https://doi.org/10.1016/j.rse.2021.112775.

Wei, J., Liu, S., Li, Z., Liu, C., Qin, K., Liu, X., Pinker, R.T., Dickerson, R.R., Lin, J., Boersma, K.F., Sun, L., Li, R., Xue, W., Cui, Y., Zhang, C., Wang, J., 2022b. Ground-level NO_2 surveillance from space across China for high resolution using interpretable spatiotemporally weighted artificial intelligence. Environ. Sci. Technol. 56, 9988–9998. https://doi.org/10.1021/acs.est.2c03834.

Wei, J., Wang, J., Li, Z., Kondragunta, S., Anenberg, S., Wang, Y., Zhang, H., Diner, D., Hand, J., Lyapustin, A., Kahn, R., Colarco, P., Da Silva, A., Ichoku, C., 2023a. Long-term mortality burden trends attributed to black carbon and $PM_{2.5}$ from wildfire emissions across the continental USA from 2000 to 2020: a deep learning modelling study. Lancet Planetary Health 7, e963–e975. https://doi.org/10.1016/S2542-5196(23)00235-8.

Wei, J., Li, Z., Lyapustin, A., Wang, J., Dubovik, O., Schwartz, J., Sun, L., Li, C., Liu, S., Zhu, T., 2023b. First close insight into global daily gapless 1 km $PM_{2.5}$ pollution, variability, and health impact. Nat. Commun. 14, 8349. https://doi.org/10.1038/s41467-023-43862-3.

Wu, H., Zhang, B., Wei, J., Lu, Z., Zhao, M., Liu, W., Bovet, P., Guo, X., Xi, B., 2022. Short-term effects of exposure to ambient PM_1, $PM_{2.5}$, and PM_{10} on ischemic and hemorrhagic stroke incidence in Shandong Province, China. Environ. Res. 212, 113350. https://doi.org/10.1016/j.envres.2022.113350.

Xia, Y., Hu, Y., Huang, Y., Bian, J., Zhao, C., Wei, J., Yan, Y., Xie, F., Lin, J., 2022. Concurrent hot extremes and high ultraviolet radiation in summer over the Yangtze plain and their possible impact on surface ozone. Environ. Res. Lett. 17, 64001. https://doi.org/10.1088/1748-9326/ac6c3c.

Xiao, Q., Geng, G., Xue, T., Liu, S., Cai, C., He, K., Zhang, Q., 2022. Tracking $PM_{2.5}$ and O_3 pollution and the related health burden in China 2013–2020. Environ. Sci. Technol. 56, 6922–6932. https://doi.org/10.1021/acs.est.1c04548.

Xing, L., Mao, X., Duan, K., 2022. Impacts of urban–rural disparities in the trends of $PM_{2.5}$ and ozone levels in China during 2013–2019. Atmos. Pollut. Res. 13, 101590. https://doi.org/10.1016/j.apr.2022.101590.

Xu, R., Tie, X., Li, G., Zhao, S., Cao, J., Feng, T., Long, X., 2018. Effect of biomass burning on black carbon (BC) in South Asia and Tibetan plateau: the analysis of WRF-Chem modeling. Sci. Total Environ. 645, 901–912. https://doi.org/10.1016/j.scitotenv.2018.07.165.

Xu, R., Wei, J., Liu, T., Li, Y., Yang, C., Shi, C., Chen, G., Zhou, Y., Sun, H., Liu, Y., 2022a. Association of short-term exposure to ambient PM_1 with total and cause-specific cardiovascular disease mortality. Environ. Int. 169, 107519. https://doi.org/10.1016/j.envint.2022.107519.

Xu, H., Yang, T., Guo, B., Silang, Y., Dai, Y., Baima, K., Gao, Y., Tang, S., Wei, J., Jiang, Y., Feng, S., Li, S., Xiao, X., Zhao, X., 2022b. Increased allostatic load associated with ambient air pollution acting as a stressor: cross-sectional evidence from the China multi-ethnic cohort study. Sci. Total Environ. 831, 155658. https://doi.org/10.1016/j.scitotenv.2022.155658.

Xu, R., Shi, C., Wei, J., Lu, W., Li, Y., Liu, T., Wang, Y., Zhou, Y., Chen, G., Sun, H., Liu, Y., 2022c. Cause-specific cardiovascular disease mortality attributable to ambient temperature: a time-stratified case-crossover study in Jiangsu province, China. Ecotox. Environ. Safe. 236, 113498. https://doi.org/10.1016/j.ecoenv.2022.113498.

Xu, R., Wang, Q., Wei, J., Lu, W., Wang, R., Liu, T., Wang, Y., Fan, Z., Li, Y., Xu, L., Shi, C., Li, G., Chen, G., Zhang, L., Zhou, Y., Liu, Y., Sun, H., 2022d. Association of short-term exposure to ambient air pollution with mortality from ischemic and hemorrhagic stroke. Eur. J. Neurol. 29, 1994–2005. https://doi.org/10.1111/ene.15343.

Xu, R., Huang, S., Shi, C., Wang, R., Liu, T., Li, Y., Zheng, Y., Lv, Z., Wei, J., Sun, H., Liu, Y., 2023. Extreme temperature events, fine particulate matter, and myocardial infarction mortality. Circulation 148, 312–323. https://doi.org/10.1161/CIRCULATIONAHA.122.063504.

Xu, L., Xu, R., Ye, Y., Wang, R., Wei, J., Shi, C., Lin, Q., Lv, Z., Huang, S., Tian, Q., Liu, Y., 2024. Short-term exposure to ambient air pollution and hospital admissions for angina among older adults in South China. Atmos. Environ. 318, 120198. https://doi.org/10.1016/j.atmosenv.2023.120198.

Xu, R., Sun, H., Zhong, Z., Zheng, Y., Liu, T., Li, Y., Liu, L., Luo, L., Wang, S., Lv, Z., Huang, S., Shi, C., Chen, W., Wei, J., Xia, W., Liu, Y., 2024a. Ozone, heat wave, and cardiovascular disease mortality: a population-based case-crossover study. Environ. Sci. Technol. 58, 171–181. https://doi.org/10.1021/acs.est.3c06889.

Xu, R., Luo, L., Yuan, T., Chen, W., Wei, J., Shi, C., Wang, S., Liang, S., Li, Y., Zhong, Z., Liu, L., Zheng, Y., Deng, X., Liu, T., Fan, Z., Liu, Y., Zhang, J., 2024b. Association of short-term exposure to ambient fine particulate matter and ozone with outpatient visits for anxiety disorders: a hospital-based case-crossover study in South China. J. Affect. Disord. 361, 277–284. https://doi.org/10.1016/j.jad.2024.06.007.

Xue, T., Zheng, Y., Geng, G., Xiao, Q., Meng, X., Wang, M., Li, X., Wu, N., Zhang, Q., Zhu, T., 2020. Estimating spatiotemporal variation in ambient ozone exposure during 2013–2017 using a data-fusion model. Environ. Sci. Technol. 54, 14877–14888. https://doi.org/10.1021/acs.est.0c03098.

Yang, J., Wang, K., Lin, M., Yin, X., Kang, S., 2022. Not biomass burning but stratospheric intrusion dominating tropospheric ozone over the Tibetan plateau. Proc. Natl. Acad. Sci. 119, e2083965177. https://doi.org/10.1073/pnas.221100211.

Yang, G., Liu, Y., Li, W., Zhou, Z., 2023. Association analysis between socioeconomic factors and urban ozone pollution in China. Environ. Sci. Pollut. R. 30, 17597–17611. https://doi.org/10.1007/s11356-022-23298-w.

Yang, Q., Zhao, T., Bai, Y., Wei, J., Sun, X., Tian, Z., Hu, J., Ma, X., Luo, Y., Fu, W., Yang, K., 2024. Interannual variations in ozone pollution with a dipole structure over eastern China associated with springtime thermal forcing over the Tibetan plateau. Sci. Total Environ. 923, 171527. https://doi.org/10.1016/j.scitotenv.2024.171527.

Yin, P., Chen, R., Wang, L., Meng, X., Liu, C., Niu, Y., Lin, Z., Liu, Y., Liu, J., Qi, J., You, J., Zhou, M., Kan, H., 2017. Ambient ozone pollution and daily mortality: a Nationwide study in 272 Chinese cities. Environ. Health Perspect. 125, 117006. https://doi.org/10.1289/EHP1849.

Yin, H., Sun, Y., Notholt, J., Palm, M., Ye, C., Liu, C., 2022. Quantifying the drivers of surface ozone anomalies in the urban areas over the Qinghai-Tibet plateau. Atmos. Chem. Phys. 22, 14401–14419. https://doi.org/10.5194/acp-22-14401-2022.

Yin, X., Rupakheti, D., Zhang, G., Luo, J., Kang, S., de Foy, B., Yang, J., Ji, Z., Cong, Z., Rupakheti, M., Li, P., Hu, Y., Zhang, Q., 2023. Surface ozone over the Tibetan plateau controlled by stratospheric intrusion. Atmos. Chem. Phys. 23, 10137–10143. https://doi.org/10.5194/acp-23-10137-2023.

Zeng, Y., Cao, Y., Qiao, X., Seyler, B.C., Tang, Y., 2019. Air pollution reduction in China: recent success but great challenge for the future. Sci. Total Environ. 663, 329–337. https://doi.org/10.1016/j.scitotenv.2019.01.262.

Zhang, J., Sun, H., Chen, Q., Gu, J., Ding, Z., Xu, Y., 2019. Effects of individual ozone exposure on lung function in the elderly: a cross-sectional study in China. Environ. Sci. Pollut. R. 26, 11690–11695. https://doi.org/10.1007/s11356-019-04324-w.

Zhang, W., Liu, D., Tian, H., Pan, N., Yang, R., Tang, W., Yang, J., Lu, F., Dayananda, B., Mei, H., Wang, S., Shi, H., 2022. Recurrent mapping of hourly surface ozone data (HrSOD) across China during 2005–2020 for ecosystem and human health risk assessment. Earth Syst. Sci. Data Discuss. 2022, 1–36. https://doi.org/10.5194/essd-2022-428.

Zhang, X., Yan, B., Zhou, Y., Osei, F., Li, Y., Zhao, H., Cheng, C., Stein, A., 2022a. Short-term health impacts related to ozone in China before and after implementation of policy measures: a systematic review and meta-analysis. Sci. Total Environ. 847, 157588. https://doi.org/10.1016/j.scitotenv.2022.157588.

Zhang, X., Osei, F., Stein, A., Cheng, C., Maji, K.J., 2022b. Temporal and spatial evolution of short-term exposure to ozone pollution: its health impacts in China based on a meta-analysis. J. Clean. Prod. 373, 133938. https://doi.org/10.1016/j.jclepro.2022.133938.

Zhang, T., Zhou, Y., Zhu, Z., Li, X., Asrar, G.R., 2022c. A global seamless 1 km resolution daily land surface temperature dataset (2003−2020). Earth Syst Sci Data 14, 651–664. https://doi.org/10.5194/essd-14-651-2022.

Zhang, F., Li, T., Chen, B., Li, N., Zhang, X., Zhu, S., Zhao, G., Zhang, X., Ma, T., Zhou, F., Liu, H., Zhu, W., 2023a. Air pollution weaken your muscle? Evidence from a cross-sectional study on sarcopenia in Central China. Ecotox. Environ. Safe. 258, 114962. https://doi.org/10.1016/j.ecoenv.2023.114962.

Zhang, L., Wang, L., Liu, B., Tang, G., Liu, B., Li, X., Sun, Y., Li, M., Chen, X., Wang, Y., Hu, B., 2023b. Contrasting effects of clean air actions on surface ozone concentrations in different regions over Beijing from may to September 2013–2020. Sci. Total Environ. 903, 166182. https://doi.org/10.1016/j.scitotenv.2023.166182.

Zhang, Y., Wei, J., Liu, C., Cao, W., Zhang, Z., Li, Y., Zeng, Q., Sun, S., 2023c. Association between ambient PM1 and semen quality: a cross-sectional study of 27,854 men in China. Environ. Int. 175, 107919. https://doi.org/10.1016/j.envint.2023.107919.

Zhang, C., Yang, J., Wei, J., Liu, Y., Zhu, H., Li, X., Wang, J., Chen, R., 2024. Individual ambient ozone exposure during pregnancy and adverse birth outcomes: exploration of the potentially vulnerable windows. J. Hazard. Mater. 464, 132945. https://doi.org/10.1016/j.jhazmat.2023.132945.

Zhao, M., Cheng, C., Zhou, Y., Li, X., Shen, S., Song, C., 2022a. A global dataset of annual urban extents (1992–2020) from harmonized nighttime lights. Earth Syst Sci Data 14, 517–534. https://doi.org/10.5194/essd-14-517-2022.

Zhao, Y., Zhang, X., Chen, M., Gao, S., Li, R., 2022b. Regional variation of urban air quality in China and its dominant factors. J. Geogr. Sci. 32, 853–872. https://doi.org/10.1007/s11442-022-1975-8.

Zhou, Z., Feng, J., 2019. Deep forest. Natl. Sci. Rev. 6, 74–86. https://doi.org/10.1093/nsr/nwy108.

Zhou, W., Wang, Q., Li, R., Zhang, Z., Wang, W., Zhou, F., Ling, L., 2023. The effects of heatwave on cognitive impairment among older adults: exploring the combined effects of air pollution and green space. Sci. Total Environ. 904, 166534. https://doi.org/10.1016/j.scitotenv.2023.166534.

Zhu, Q., Bi, J., Liu, X., Li, S., Wang, W., Zhao, Y., Liu, Y., 2022. Satellite-based Long-term spatiotemporal patterns of surface ozone concentrations in China: 2005–2019. Environ. Health Perspect. 130, 27004. https://doi.org/10.1289/EHP9406.